Global River Delta Morphology: Predictions Versus Observations within the Galloway Ternary Diagram

Juan F. Paniagua-Arroyave[1,2,3*], Jaap H. Nienhuis[2]

[1] Area of Natural Systems and Sustainability, Hydrology of Northern Andes (HyNA) Group, School of Applied Sciences and Engineering, EAFIT University, Colombia

[2] Department of Physical Geography, Faculty of Geosciences, Utrecht University, The Netherlands

[3] INSTAAR, University of Colorado Boulder, USA

Corresponding author: Juan F. Paniagua-Arroyave, Escuela de Ciencias Aplicadas e Ingeniería, Universidad EAFIT (jpaniag2@eafit.edu.co)

Key points:

- We propose a quantitative ternary diagram of delta morphology to compare predictions with observations.
- Prediction error is lowest for tide-influenced deltas, and higher for mixed-influenced deltas.
- The deviation between observations and predictions can indicate delta plain sediment retention.

Abstract

Waves, rivers, and tides play a leading role in shaping delta morphology. Recent studies have enabled predictions of their relative influence for deltas globally, but methods and associated uncertainties have remained poorly described. Here we aim to address that gap and assess the quality of delta morphology predictions compared to observations for 31 deltas globally. We expand on seminal works that quantified the Galloway ternary diagram from the balance between river, wave, and tidal sediment fluxes. Our data includes uncertainties for delta shoreline protrusion angles set by wave influence (14.1°±12° predicted vs. 20.8°±16.1° observed), channel widening, set by tidal influence (53.5±170.8 predicted vs. 6.5±11.5 observed), and number of distributary channels, set by river influence (55.9±127.5 predicted vs. 21.4±43.0 observed). Within the ternary diagram for delta morphology, we find an average error of 8% (±11%, 1 standard deviation), linked to uncertainties in wave and tide sediment fluxes. Relative uncertainties are greatest for mixed-process deltas (e.g., Sinu, error of 49%) and tend to decrease for end-member morphologies where either one of wave, tide, or river sediment fluxes dominates (e.g., Fly, error of 0.2%). Large sources of prediction uncertainties are (1) delta morphology data, e.g., delta slopes that modulate tidal fluxes, (2) data on river sediment flux distribution between individual delta river mouths, and (3) theoretical basis behind fluvial and tidal dominance. Future work could help address these three sources and improve predictions of delta morphology.

Plain Language Summary

Waves, rivers, and tides determine the shape of deltas, and, because of their intricate relations, it is very difficult to predict how much delta shape changes. Recent works have attempted this but fall short in describing the methods and quantifying the accuracy. Here we propose a new way of predicting delta shape by means of the Galloway triangle. We apply our new method to 31 deltas, picked by us by looking for shape diversity. By “delta shape” we mean “delta pointiness”, how many channels the delta has, and how wide they are. We get an average error of 8%, with a maximum of 49% (Sinu delta) and a minimum of 0.2% (Fly delta). We find small uncertainties for “extreme deltas” (e.g., Mississippi, Eel, Elbe) and large uncertainties in prediction for

deltas controlled by a combination of processes (e.g., Sinu). To improve our predictions, we must get better morphology data, account for sediment distribution among delta distributary mouths, and refine our theoretical presumptions.

1. Introduction

The sustainable development of coastal communities depends upon our ability to predict future coastal morphological changes, particularly at deltas. Deltas exists at the confluence of marine and terrestrial sediment fluxes, which creates highly dynamic land-ocean (coastal) environments and make predictions particularly challenging.

The aim of this study is to test delta morphology predictions from a new quantitative ternary diagram (Nienhuis et al., 2020), based on one originally proposed by Galloway (1975). This new ternary diagram enables predictions of (1) delta shoreline protrusion, (2) downstream channel widening, and (3) the number of distributary channels, all based on the sediment flux balance between the river, waves, and tides.

The original study made predictions of delta morphology and evaluated whether it matched with observed morphologic dominance by of one of these sediment fluxes. Here, we expand the original study and retrieve observations of morphological characteristics for 31 deltas and test the predicted morphologic influence. We also discuss sources of prediction uncertainties with implications for delta plain sediment retention efficiency within deltas worldwide.

2. Background

2.1. Delta Morphology as a Product of its Environment

Deltas arise within the river source-to-sink sediment path (Bentley et al., 2016; Liu et al., 2009) when rivers debouche into a basin and their capacity for sediment transport is reduced (Gilbert, 1885). Resulting deposits create topsets, foresets, and bottomsets, with morphologies shaped by a combination of terrestrial and marine processes (Patruno & Helland-Hansen, 2018; Wang et al., 2011). Terrestrial processes include rivers that mold mouthbars, create crevasse splays, and avulse channels, and whose morphologic effects are evident in the resulting distributary channel geometry and networks (Coffey & Shaw, 2017; Shaw et al., 2013), further affected by vegetation, waves, and tides (Nienhuis et al., 2015; Passalacqua et al., 2013).

The sediment fraction that does not deposit at delta foresets and topsets continues its transit to the basin's bottom with an analogous set of dynamics controlling submarine deposits (e.g., Jobe et al., 2015; Naranjo-Vesga et al., 2020; Reading & Richards, 1994). These rich subaerial and submarine dynamics have long challenged predictions of delta morphology (Fagherazzi & Overeem, 2007; Gao et al., 2011; Olliver et al., 2020).

2.2. Where We Came From: Characterizing Delta Morphology

The seminal work that conceptualized delta morphology in relation to terrestrial and marine processes includes Galloway's (1975), with the ternary diagram of delta morphology. In it, deltas result from the relative effect of the river, tides, and waves on morphology. River-dominated deltas attain a "bird-foot" morphology because to dominance of fluvial over marine fluxes enables mouth bar formation and maintenance of multiple distributary channels (Coleman & Wright, 1975; Ke et al., 2019; Wolinsky et al., 2010; Wright, 1977). Conversely, waves tend to redistribute sediments near river mouths by alongshore and cross-shore fluxes caused by spatial gradients in wave breaking (Komar, 1973). This process flattens shorelines and can seal of river mouths (Jerolmack & Swenson, 2007; Nienhuis et al., 2015). Tides, as the third major process, create in- and outflow of water and sediments in river mouths and lead to estuarine morphologies

(Dalrymple et al., 1992; Goodbred & Saito, 2012; Valle-Levinson, 2010). Delta morphologies also exist where there is a mix of fluvial and marine fluxes (e.g., Sinu).

Inherent to Galloway's diagram and other works (Postma, 1995; Wright & Coleman, 1973) is the realization of a morphologic continuum of river deltas and the existence of river, tide, and wave-dominated end members. These end members include the traditional "bird-foot" deltas as river-dominated, funnel-shaped alluvial estuaries (e.g., Fly) and rivers mouths with straight shorelines (e.g., Eel, and many other small deltas) as tidal and wave end members. However, end members have traditionally not been well-defined, leading to extensions of the ternary diagram toward strandplains, tidal flats, and estuaries (Boyd et al., 1992; Nienhuis et al., 2020).

Other challenges that arose from Galloway's diagram relate to quantifying the river, waves, and tides processes, and their effect on delta morphology. Each process was usually represented independently by quantitative expressions that were assumed to be relevant for modifying delta morphology. For example, waves' potential to redistribute sediments alongshore were represented by wave power (Wright & Coleman, 1971, 1972), but comparison with similar river- and tidal power proved difficult. Resulting delta morphology was described as estuarine, lobate, or cuspate, but was not quantified in morphometrics.

2.3. Where We Are Now: Predicting Delta Morphology

Recent studies explored the quantification of the Galloway's ternary relation as an integral predictive framework, i.e., with a physical coupling between the river, tides, and waves, and delta morphology (Baumgardner, 2016; Konkol et al., 2022; Overeem et al., 2022; Seybold et al., 2007; Woodroffe et al., 2006 and others). In this vein, Nienhuis et al. (2020) proposed a quantitative framework of how much fluvial, wave, and tidal fluxes influence delta morphology.

A quantitative characterization of Galloway's ternary diagram consists of three steps. First, it requires a definition of the morphological characteristics that define each of the ternary axes. Wave dominance expresses itself through cuspate shorelines with a plan-view shoreline protrusion that decreases with increasing wave influence. There is a high likelihood for littoral spit formation (Ashton & Giosan, 2011; Broaddus et al., 2022;

Dan et al., 2011) and alongshore sediment bypassing (Nienhuis et al., 2016). Tidal dominance expresses itself as the downstream channel widening near river mouths, as nearshore morphology must accommodate transient volumes of water moved by tides (Nienhuis et al., 2018). Fluvial dominance expresses itself by the absence of downstream channel widening, the absence of straight shorelines, and the appearance of distributary channels (Nienhuis et al., 2015).

The second step is to understand how wave, tidal, and river processes make these delta morphological characteristics. New theory enabled quantitative relations between downstream channel widening and shoreline orientation as a function of fluvial sediment loads toward river mouths and wave-driven and tide-driven sediment loads away from river mouths, all in terms of a mass rate of sediment (Nienhuis et al., 2015, 2018).

In a third step, the sediment mass flux rates at the river mouth are predicted using formulations of only upstream fluvial characteristics and offshore tidal and wave characteristics. Although river, wave, and tidal sediment fluxes can be measured directly in the field, such measurements are sparse. An a-priori prediction, based on wave, tidal, and river boundary conditions, enables the use of widely (globally) available data. These boundary conditions can then be reformulated into a capacity to move sediments near river mouths, and then further toward the resulting delta morphology.

The quantitative ternary diagram supports a continuum of coastal morphologies of all ratios of wave, tide, and river sediment fluxes. There is no inherent lower limit to the fluvial sediment flux, even though the term river delta become increasingly incorrect for vanishingly small river sediment deposits. This limitation was recognized before by Dalrymple et al. (1992) and Boyd et al. (1992) in their attempt to quantify coastal alluvial morphologies. The quantified ternary diagram can therefore also be thought of as characterizing a collection of coastal morphologies that includes deltas, strandplains, and estuaries, although no quantitative criteria exist, yet, to separate these morphologies.

Another implication of the quantified ternary approach is that it is based on a sediment flux balance and therefore includes the effects of sediment characteristics on delta morphology (Edmonds & Slingerland, 2010). For example, the effect that coarser grain size leads to increased topset delta slopes and reductions in tidal dominance is

included in the formulation for the tidal sediment flux. Earlier energetics-based approaches did not include grain size and therefore required added dimensions in the ternary space (Orton & Reading, 1993).

A downside of the quantified ternary approach is that it is based on the fluvial sediment flux at the river mouth – data which may be difficult to acquire. Channel bifurcations reduce the fluvial sediment flux at individual river mouths compared to the delta apex (for which data is most often available). The tidal sediment flux depends on the tidal prism, which decreases as channels split and become narrower, but not linearly with the number of distributary channels (Nienhuis et al., 2018; Sassi et al., 2011). The wave sediment flux acts on each river mouth. Deltas can therefore bifurcate themselves into tide- or wave-dominance.

Similarly, fluvial sediment trapping on delta plains upstream of river mouths and sediment bypassing offshore of river mouths may also reduce the fluvial sediment available for redistribution at the river mouth. Estimates for some deltas suggest that ~30% of the fluvial sediment load may be trapped on delta plains (Paola et al., 2011). A possible additional effect of sea-level rise on sediment trapping and delta morphology has been included in the quantified ternary approach (Nienhuis et al., 2023; Nienhuis & van de Wal, 2021), but, because of limited data, has not been widely adopted.

2.4. The Next Step: Quantifying Sources of Prediction Uncertainty

The quantified ternary approach presents a theoretical advance of deltas and a reasonable step toward a global predictive model of delta morphology (Hoitink et al., 2020). But how accurate is it? A categorical comparison with observations, i.e., whether observed wave-dominated deltas were predicted to be wave dominated, shows that 85% of the deltas (265 out of 312) are classified correctly (Nienhuis et al., 2020). Whether or not the delta morphological characteristics of channel widening, shoreline protrusion, and the number of distributary channels, are predicted accurately within the ternary diagram remains an open question.

This study compares delta morphologic predictions to observations, i.e., predicted versus observed delta location within the ternary diagram based on channel widening, shoreline protrusion, and the number of distributary channels. We use two sets of deltas:

a set of well-known international examples (Best, 2019; Galloway, 1975; Nienhuis et al., 2020) along with another set of deltas draining the Northern Andes (Restrepo & López, 2008). Our approach's key advance consists of providing a methodology for representing delta morphology from first-order morphological observations within the framework of morphology predictions (Nienhuis et al., 2020). We show that some of the discrepancy between predictions and observations could relate to the partitioning of fluvial sediment delivery between the delta plain and delta coast, in several cases strongly modified by humans.

3. Methods

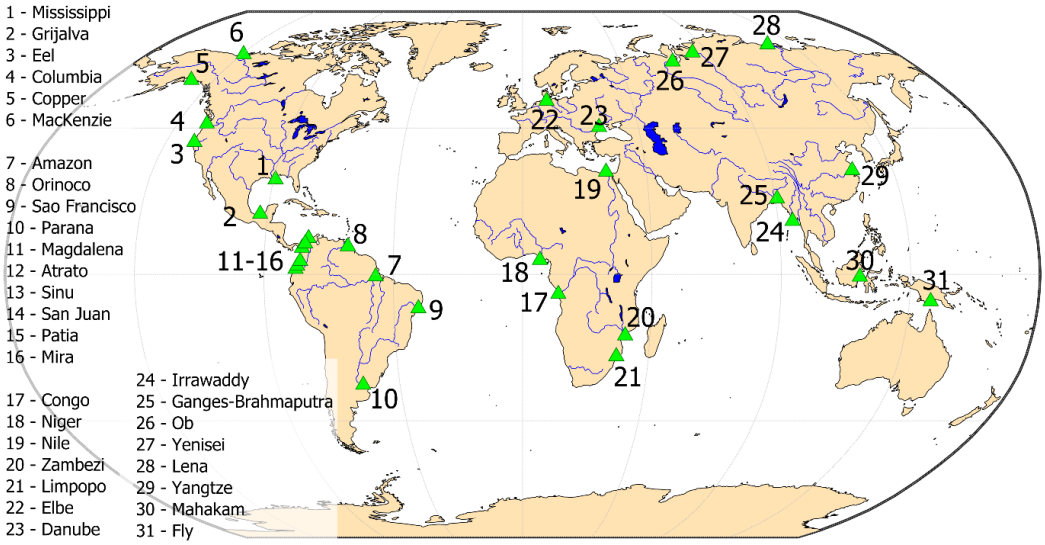

Figure 1. Location of 31 deltas assessed in this study, in North America, South America, Africa, Europe, Asia, and Oceania. Delta numbers 11-16 correspond to the Northern Andes deltas (see Figure 2 for their location).

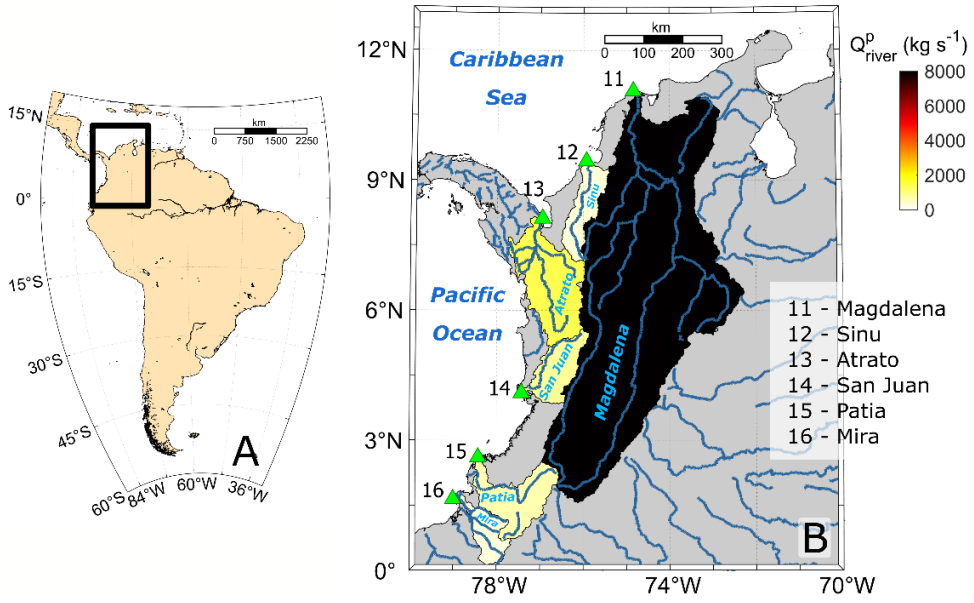

Figure 2. Location of Northern Andes deltas (11-16) in the Colombian coastal zone marked by green triangles in (A) South America and (B) showing main streams, catchment areas, and pristine fluvial sediment flux (Q^p_{river}).

We predict and observe the morphology of 31 deltas. This selection aims to represent a range of morphologies and also contains some of the largest fluvial catchments (Best, 2019; Galloway, 1975; Nienhuis et al., 2020; Restrepo & López, 2008) (Figure 1 and Figure 2). For every delta, we predict its morphology from the fluvial sediment flux at the delta apex and offshore wave and tidal characteristics. Then, we compare our predictions to observations of modern delta morphology. For this comparison we introduce an error metric based on the distance between the predicted and observed position of a delta within the delta ternary diagram.

3.1. Delta Morphology Predictions

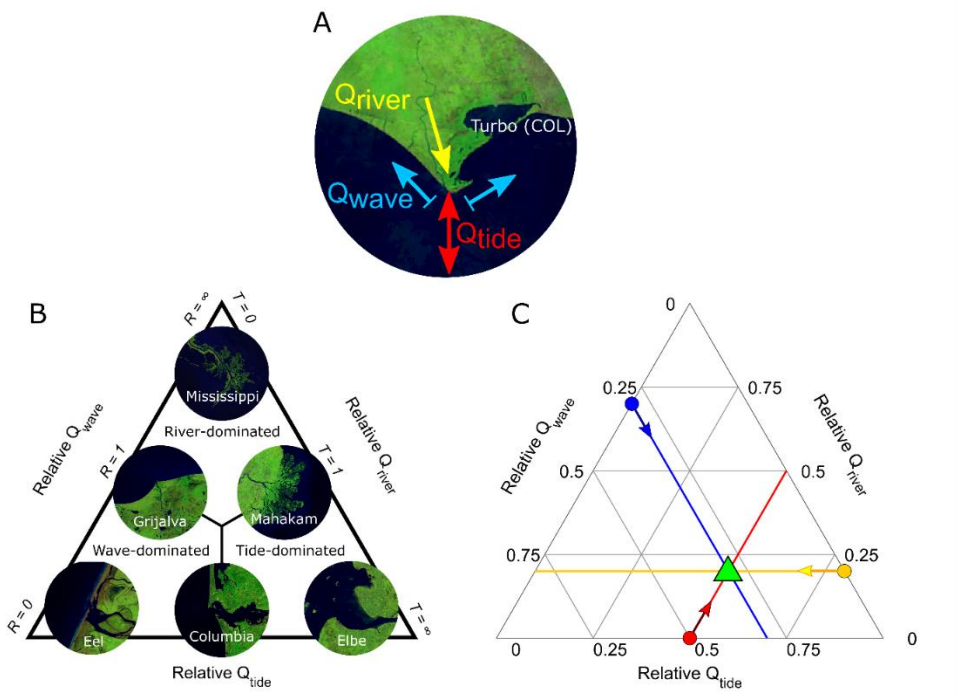

Figure 3. (A) Schematic of sediment flux balance by river, waves, and tides at Turbo River delta, Colombia. Imagery by Aquamonitor (Donchyts et al., 2016, https://aqua-monitor.appspot.com/). (B) Galloway's ternary diagram showing the dominance ratios R and T within the context of relative sediment fluxes and end-member delta morphologies. Modified from Nienhuis et al. (2020, Fig. 1a) with imagery by Aquamonitor. (C) Location of a hypothetical delta in the ternary diagram, with relative fluxes, $r_{river} = 0.2$ (yellow), $r_{wave} = 0.3$ (blue), and $r_{tide} = 0.5$ (red). The intersection (green triangle) shows the location of the hypothetical delta within the ternary diagram. Red, blue, and yellow arrows indicate the direction for drawing lines of constant values of corresponding r_x values.

We applied the Nienhuis et al. (2020) methodology that predicts delta morphology from the balance of fluvial, wave, and tide sediment fluxes (Figure 3A). This approach uses a tripartite relative sediment flux Q_x, referred to as r_x (where x corresponds to $river$, $wave$, or $tide$). The relative flux represents the dominance of riverine, wave- and tide-related sediment fluxes at the river mouth as a fraction of their sum, as

$$r_{river} = \frac{Q_{river}}{Q_{river}+Q_{wave}+Q_{tide}},$$

$$r_{wave} = \frac{Q_{wave}}{Q_{river}+Q_{wave}+Q_{tide}}, \quad (1)$$

and

$$r_{tide} = \frac{Q_{tide}}{Q_{river}+Q_{wave}+Q_{tide}},$$

such that $r_{tide} + r_{wave} + r_{river} = 1$, with the sediment fluxes defined below. Each ratio represents the fraction of the total sediment flux that each process contributes. For example, if all processes move the same quantity of sediments, then $r_{river} = r_{wave} = r_{tide} = 0.\overline{3}$. For a delta with $r_{river} = 0.2$, $r_{wave} = 0.3$, and $r_{tide} = 0.5$ (Figure 3B), we locate values along its axis and draw a line following the arrows. Once we get the relative sediment fluxes, we obtain the process dominance by plotting these relative fluxes within a ternary diagram. Each relative flux corresponds to an axis within the chart, and dominances reflect delta morphology according to each axis (Figure 3B).

Variations in delta morphology along one dimension (e.g., from river to tide dominance or wave to river dominance) have been previously quantified by the fluvial (R) and tidal (T) dominance ratios. These 1-dimensional factors have a straightforward relation to their 2-dimensional ternary cousins as

$$R = \frac{Q_{river}}{Q_{wave}} = \frac{r_{river}}{r_{wave}}, \quad (2)$$

249

250 and

251

$$T = \frac{Q_{tide}}{Q_{river}} = \frac{r_{tide}}{r_{river}}, \quad (3)$$

252

253 as given by Nienhuis et al. (2015, 2018).

254 The R factor represents river-to-wave dominance by comparing the riverine
255 sediment discharge (Q_{river}) to the maximum potential sediment transport by waves
256 alongshore away from the river mouth (Q_{wave}). In this case, high wave dominance (low
257 R) results in a straight coastline. Increasing fluvial dominance leads to greater delta
258 protrusion.

259 Similarly, the T factor represents tide dominance by comparing the amplitude of
260 tidal sediment discharge at the river mouth (Q_{tide}) to the fluvial sediment discharge
261 (Q_{river}). Tidal dominance (T>1) results in flow reversal at the river mouth, and
262 downstream widening of the river channel, an estuarine “funnel” morphology, whereas
263 T<1 results in small downstream tide-driven change in river mouth width (Nienhuis et al.,
264 2018).

265

266 ***3.1.1. Estimating Q_{wave}***

267

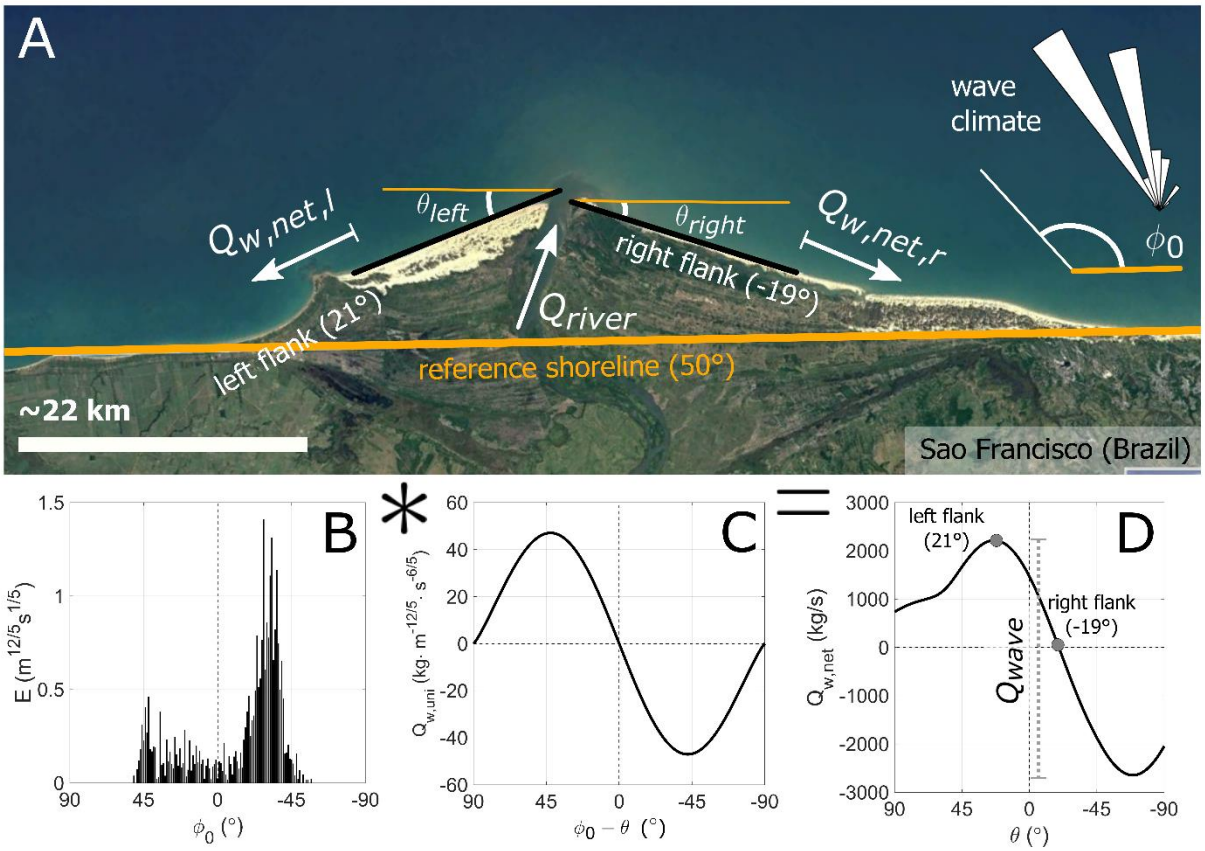

Figure 4. Computing $Q_{w,net}$ and Q_{wave} for the Sao Francisco River delta, on the Brazilian coast. (A) Sao Francisco delta showing morphology and wave climate distribution. We obtained flank angles from Google Earth® imagery (ϕ_0, θ_{left}, and θ_{right} in ° with respect to the reference shoreline). (B) Wave energy distribution as a function of wave approach angle from Wavewatch simulations (Chawla et al., 2013). (C) Unitary-wave alongshore transport as a function of wave-to-shoreline approach angle. (D) Net alongshore sediment transport as a function of shoreline angle. Gray dots show net transport expected at left and right flanks ($Q_{w,net,l}$ and $Q_{w,net,r}$). The bar shows the wave sediment flux range (Q_{wave}) that the left and right flanks must pass through to become river dominated. Symbols between panels B through D (asterisk and equal) represent the convolution operation to quantify $Q_{w,net}$ (see text).

Q_{wave} represents the maximum potential alongshore sediment flux by waves away from the river mouth along any shoreline angle (in kg s^{-1}). It is the sum of the maximum potential transport to the right and left from the river mouth (Nienhuis et al., 2015 their Supp. Info.) (Figure 4). It can be derived from wave climate analysis alone and it does not require delta morphology observation beyond a reference shoreline orientation at the delta. Q_{wave} is given by

285

$$Q_{wave} = \max\left[Q_{w,net}(\theta)\right]_{-\pi\leq\theta\leq 0} - \min\left[Q_{w,net}(\theta)\right]_{0\leq\theta\leq\pi}, \quad 4$$

286

287 where the observed net alongshore sediment transport, $Q_{w,net}$, for a given
288 shoreline angle θ equals to the convolution of the mean wave-energy angle distribution,
289 $E(\phi_0)$, and the alongshore sediment transport for a unitary wave from a single direction,
290 $Q_{w,uni}(\phi_0 - \theta)$,

291

$$Q_{w,net}(\theta) = E(\phi_0) * Q_{w,uni}(\phi_0 - \theta), \quad 5$$

292

293 where the operator $[*]$ indicates convolution, $\theta \in \left(-\frac{\pi}{2}, \frac{\pi}{2}\right)$ is the angle of potential
294 delta shorelines with respect to the general shoreline orientation, θ_{shore} (so 0° is a
295 shoreline aligned with the reference shoreline, and –90° and 90° are shorelines
296 perpendicular to the reference shoreline), and ϕ_0 is the deep-water wave approach angle
297 with respect to θ_{shore} (Figure 4). The difference $\phi_0 - \theta$ refers to the angle of the wave
298 approach relative to the delta flank shoreline.

299 We calculated the wave energy $E(\phi_0)$, in $m^{12/5}s^{1/5}$, as:

300

$$E(\phi_0) = \frac{\sum_{\phi_0}\left[H_s^{12/5}(\phi_0)T^{1/5}(\phi_0)\right]}{N}, \quad 6$$

301

302 where H_s (m) is the significant wave height, and T (s) is the wave period, and N is
303 the number of observations. In addition, we calculated the alongshore sediment transport
304 distribution, $Q_{w,uni}$ (in $kg \cdot m^{-12/5}s^{-6/5}$), based on the alongshore sediment transport
305 function (Ashton & Murray, 2006 Eq. 5) for unitary offshore (or un-refracted) wave energy,
306 i.e., for $H_s = 1\ m$ and $T = 1\ s$, as

307

$$Q_{w,uni} = K\rho_s(1-p)\cos^{6/5}(\phi_0 - \theta)\sin(\phi_0 - \theta), \quad (7)$$

308

309 where $K \approx 0.06\, m^{3/5}s^{-6/5}$ is an empirical constant (Nienhuis et al., 2015) $\rho_s =$
310 $2{,}650\ kg/m^3$ is the assumed density of sediments, and $p = 0.4$ is their dry mass void
311 fraction.

312 Alternatively, if no distribution of wave approach angles is available, there is also
313 a simpler approach to estimate Q_{wave}. This function assumes that waves approach is
314 perpendicular to the delta shoreline, such that there is no wave sheltering and the
315 maximum (to the right) and the minimum (to the left) transport have the same absolute
316 magnitude. The maximum potential transport away from the river mouth (Q_{wave}) is then

317

$$Q_{wave} \approx 2 \cdot K\rho_s(1-p) \cdot H_s^{\frac{12}{5}} \cdot T^{\frac{1}{5}} \cdot 0.47. \quad (8)$$

318

319 In this study, for all 31 deltas, we retrieve a 30-year record of H_s, T, and ϕ_0 from
320 the WaveWatch III reanalysis (Chawla et al., 2013) for a computational node closest to
321 each delta and apply Eq. 4 to estimate Q_{wave} (Nienhuis et al., 2020).

322

323 ***3.1.2. Estimating Q_{tide}***

324

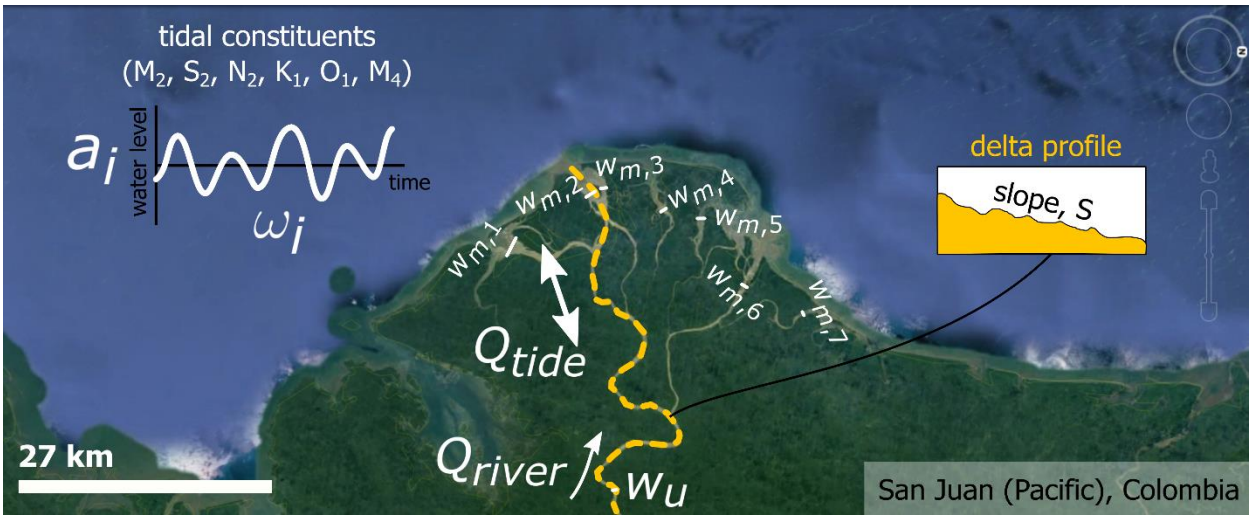

Figure 5. Metrics involved in the calculation of sediment flux by tides, Q_{tide}, from delta morphology, as given for the San Juan River delta (Colombia). In this case, there are seven distributary mouths, with a channel width for each mouth ($w_{m,1}$, etc., also applied for fluvial-dominated deltas), measured from the Google Earth® imagery. We calculated the delta slope with an average of elevation change and distance along the transect in yellow. We represent tidal properties by amplitudes and frequencies of tidal constituents. We use Q_{river} to quantify fluvial channel depth (see text for explanation).

We calculated Q_{tide}, defined as the tide-driven sediment flux amplitude (kg s^{-1}) at the river mouth, for the largest tidal constituent (giving the average tidal amplitude) as

$$Q_{tide} = \frac{1}{2}\omega k a^2 L^2 \beta f c, \qquad 9$$

where a is the offshore tidal amplitude in meters, $k = \omega\left(\sqrt{\Theta_c D_{50}} R C_z \pi\right)$ is a sediment transport coefficient in m^{-1}, ω is the tidal angular frequency in radians per second, Θ_c $(= 0.2)$ is the Shields number for sediment motion, D_{50} $(= 0.1\,mm)$ is the median grain size, R $(= 1.65)$ is the submerged specific gravity of sediment, C_z $(= 55)$ is a Chézy roughness coefficient, L is a characteristic estuarine length (or estuary length, defined as d/S), $\beta = \frac{w_u}{d}$ is the fluvial channel aspect ratio (w_u is the fluvial channel width and d the channel depth), $f = 1 + \frac{2S}{ka}$ (with S as the mean delta channel slope), c is the sediment concentration (kg m^{-3}), assumed equal to the river sediment concentration,

derived from the mean annual sediment flux Q_{river} (kg s^{-1}), and the mean annual water discharge (in m^3/s) (Figure 5).

We estimate channel depth following hydraulic geometry and a constant aspect ratio. In addition, we measured delta slope (S) from Google Earth's imagery and SRTM elevation data and combined them with tidal constituent data (Egbert & Erofeeva, 2002, https://jhnienhuis.users.earthengine.app/view/changing-shores).

Overall, channel widening will increase for more significant tidal fluxes relative to the fluvial fluxes. Also, it will grow for low delta slopes relative to half the tidal velocity ($\frac{1}{2}\omega a$) and high slopes relative to the tidal wave steepness (ka). This intricate relationship is represented by the variation of channel widening with T in Figure 6B.

3.1.3. Estimating Q_{river}

Q_{river} represents the mean fluvial sediment flux toward the delta at the delta apex. We estimate Q_{river} as the long-term (>30 years) average suspended sediment load from the WBMSed 2.0 model (Cohen et al., 2014) as a spatially discretized BQART model (Syvitski & Milliman, 2007) as

$$Q_{river} = \chi B Q_{w,River}^{0.3} A^{0.5} R_r t, \text{ for } t \geq 2\ ^\circ C,$$

or (10)

$$Q_{river} = 2\chi B Q_{w,River}^{0.3} A^{0.5} R_r t, \text{ for } t < 2\ ^\circ C,$$

where $\chi = 0.02$, $B(= IL[1 - T_E]E_h)$ accounts for geological and anthropogenic factors (with I representing glacial erosion, L lithology, T_E trapping by reservoirs, and E_h human-related soil erosion), A is the drainage basin area (in km^2), R_r is the relative relief (km), t is the average temperature of the drainage basin (°C), and $Q_{w,river}$ is the average discharge (m^3/s) calculated with the WBMplus discharge model including floodplain reservoir effects (Cohen et al., 2014 and references therein).

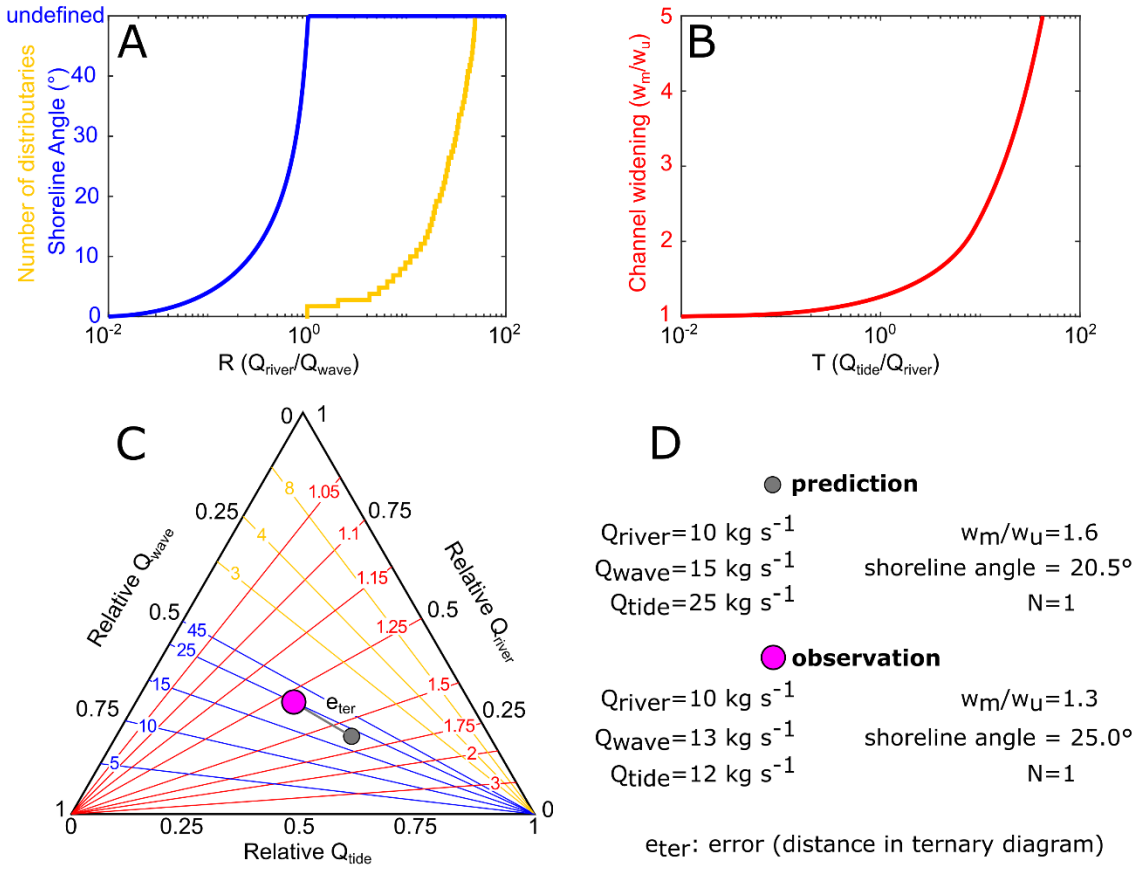

Figure 6. Relations between the delta sediment balance and its morphology within the ternary diagram. (A) Variation in shoreline angle and number of distributary mouths as a function of the fluvial dominance ratio R, for an example wave climate and following Eq. 11. Note that the relation will deviate for different wave climates. (B) Variation in downstream channel widening with the tidal dominance ratio T, for a single dominant constituent and a delta slope. Note that the relation will deviate in case of different tidal properties and channel slopes. (C) Morphological predictions cast into the ternary diagram, with contour lines and numbers indicating (in blue) shoreline angle, (in yellow) number of distributary channels, (in red) channel widening. (D) Example predictions (in grey) and observations (in purple), with $Q_{river} = 10\ kg\ s^{-1}$, $Q_{wave} = 15\ kg\ s^{-1}$, and $Q_{tide} = 25\ kg\ s^{-1}$, for which we predict a 20.5° protrusion angle, channel widening of 1.6 (mouth is 60% wider than the upstream channel), and a single distributary mouth ($R < 1$). The purple circle shows the hypothetical delta morphology observations (widening of 1.3, shoreline angle of 25°, and 1 distributary channel). Error (e_{ter}) corresponds to the distance between predictions and observations.

3.1.4. Resulting predictions

From our estimates of Q_{wave}, Q_{river}, and Q_{tide}, we predict R (Eq. 2) and T (Eq. 3) and generate a predicted delta morphology. We predict 3 morphological characteristics: the delta shorelines angles, the number of distributary channels, and the river mouth channel widening (Figure 4).

If $R < 1$ ($Q_{river} < Q_{wave}$), then all delivered river sediment is transported alongshore along both delta flanks, and therefore equal to the difference between the wave-driven alongshore fluxes (Figure 4D). Because the alongshore flux depends on the wave approach angle, this condition can be rewritten into a prediction for the flank shoreline angles. If the wave approach is symmetric, then each flank shoreline angles conveys half the fluvial sediment flux, and θ^{pred} (in °) is

$$\theta^{pred} \approx Q_{w,net}^{-1}\left(\pm\frac{1}{2}Q_{river}\right),\ R < 1. \quad (11)$$

There is no straightforward way to deconvolve $Q_{w,net}$ and solve this inverse equation analytically, but there is a simple numerical or graphical solution which involves finding the shoreline angles where $Q_{w,net} = \pm 0.5\, Q_{river}$ (Figure 4A).

Alternatively, Eq. 11 can be further simplified if there is a low directional spread in the wave approach (Figure 6A). In this case,

$$\theta^{pred} \approx \frac{1}{2}\arcsin\left(\frac{Q_{river}}{Q_{wave}}\right) = \frac{1}{2}\arcsin(R),\ R < 1. \quad (12)$$

In the case of $R > 1$, Eq. 11 and 12 are undefined and there is no shoreline angle possible that would convey the fluvial sediment flux. We then predict a river dominated delta and θ^{pred} is undefined (Figure 6A). Instead, we predict the number of distributary mouths. In the original framework (Nienhuis et al., 2015, 2018), the fluvial dominance ratio R did not provide morphological predictions for river-dominated deltas ($R > 1$). Here

409 we add a prediction on the number of distributary mouths, following other recent
410 contributions (Broaddus et al., 2022).

411 If $R > 1$ (river dominated), waves cannot move all the fluvial sediment away from
412 the river mouth. Mouthbars will form that will split the channel and create multiple river
413 mouths. The fluvial sediment flux is distributed between the mouths, whereas the potential
414 alongshore sediment flux remains the same. We therefore predict that the process of
415 mouth bar and distributary channel formation continues until the number of distributaries,
416 N_{dist}^{pred}, reaches

417

$$N_{dist}^{pred} = \lceil R \rceil,\ R > 1, \tag{13}$$

418

419 in which case each river mouth provides enough sediment to be in balance with
420 alongshore sediment transport away from the river mouth.

421 Finally, for tides, we predict the downstream channel widening, w_m/w_u as

422

$$\left.\frac{w_m}{w_u}\right|^{pred} = \frac{Q_{tide}}{Q_{river}Uf} + 1 = \frac{T}{Uf} + 1, \tag{14}$$

423

424 where $U = \frac{0.5\omega a}{S \cdot u_{river}}$ is the strength of the tidal flow of the largest tidal constituent
425 relative to the fluvial flow (u_{river}) with the quantities defined as in Eq. 9 and Nienhuis et
426 al. (2018). Funnel-shaped deltas, i.e., alluvial estuaries (e.g., Elbe), are predicted to have
427 $w_m \gg w_u$ (thus a relatively large T), whereas deltas with negligible tidal influence (e.g.,
428 Grijalva) should have $w_m \approx w_u$ (thus $T \approx 0$). We include the relations between tidal
429 dominance and morphology in Figure 6B and C, for an example *U* and *f*.

430

3.2. Delta Morphology Observations

We compare our predictions of delta morphology with observations from aerial imagery from Google Earth Pro®. For 31 deltas, we retrieved the shoreline angles, the number of distributary channels, and the river mouth and upstream channel widths (all available in the supplementary materials).

Shoreline angle observations (θ^{obs} and θ_{shore}) were retrieved by digitizing each mouth flank and reference shoreline with a straight line, i.e., by marking two points from right to left looking offshore and calculating the azimuth angle.

We obtained the difference angle between the reference shoreline and shoreline flanks, $\theta_{shore} - \Theta$, from the scalar product between the reference shoreline vector ($\overrightarrow{RS}$) and each (left and right) flank vector ($\overrightarrow{DF}$) as

$$\theta_{shore} - \Theta = \operatorname{acos}\left(\frac{\overrightarrow{RS}\cdot\overrightarrow{DF}}{RS\cdot DF}\right), \quad (15)$$

where Θ represents the delta flank azimuth, and θ_{shore} the reference shoreline azimuth. We calculate θ^{obs} from the difference angle to then quantify the alongshore sediment flux along left and right delta flanks (Figure 4).

We cast the difference angle into one of three quadrants depending on the flank (whether left or right), such as each quadrant represents a morphodynamic state: cuspate, crenulated, or estuarine.

The cuspate condition refers to the typical delta shape with straight delta flanks protruding seaward toward the river mouth. For the left flank, a cuspate delta would render a difference angle between 90 and 180° (i.e., 0 to 90° counterclockwise), then $\theta^{obs} = 180° - (\theta_{shore} - \Theta)$. Conversely, for the right flank a cuspate shoreline would render a difference angle between 0 and –90° (i.e., 0 to 90° clockwise), then $\theta^{obs} = -(\theta_{shore} - \Theta)$.

The crenulated condition occurred when we observed a river dominated delta with several distributaries ($N_{dist} > 1$) and without straight flanks. In this case, both θ^{obs} are

undefined. Although in some cases θ^{obs} can be defined for deltas for multiple distributaries (e.g., Nile, Grijalva), it is difficult to incorporate it into our ternary framework because it would make a delta simultaneously river- and wave-dominated. A lobe-based analysis is a possible solution, but this would be a departure from the rest of our analysis and therefore not undertaken here.

The estuarine conditions occurred when delta flanks protruded landward instead of seaward as the typical delta cuspate, such as the delta shape resembles the "funnel" shape (seaward increase in channel width) of single thread tide dominated deltas (e.g., Elbe). For the left flank, an estuarine delta would render a difference angle between –180 and –270° (i.e., 0 to 90° clockwise), then $\theta^{obs} = -[(\theta_{shore} - \Theta) - 180°]$. Conversely, for the right flank an estuarine shoreline would render a difference angle between –270 and –360° (i.e., 0 to 90° counterclockwise), then $\theta^{obs} = -[360° - (\theta_{shore} - \Theta)]$.

Note that we could include a "spit" condition (the fourth quadrant) when the flanks form an "inverse funnel" shape such that channel width decreases seaward, like in a funnel shaped distributary with nearshore spits narrowing the outlet. But such a condition arises when the channel is not fully alluviated and therefore it does not fit in our ternary diagram. We excluded it.

In addition to the flank angles, we counted the number of distributary mouths (N_{dist}^{obs}) and measured each river mouth width by digitizing a straight line perpendicular to the delta distributary banks closest to the ocean. We obtained the channel widening fraction $\left.\frac{w_m}{w_u}\right|^{obs}$ by calculating a single distributary mouth width from the sum of distributary widths as $w_m = \left(N_{dist}^{obs}\right)^{-0.5} \sum_{n=1}^{N_{dist}^{obs}} w_{m,n}$ (Nienhuis et al., 2018) (Figure 5) and comparing it to the upstream channel width, w_u, where the effects of tides were not evident or the channel width appeared relatively constant.

3.2.1. Observed Fluvial Dominance

We can cast the delta morphology observations into observations for the river dominance ratio (R^{obs}) and the tide-dominance ratio (T^{obs}). First,

484

$$R^{obs} = N_{dist}^{obs},\ N_{dist}^{obs} > 1,$$

or

$$R^{obs} = \frac{Q_{w,net}^{obs}}{Q_{wave}} = \frac{Q_{w,net}(\theta_{right}^{obs}) - Q_{w,net}\left(\theta_{left}^{obs}\right)}{Q_{wave}},\ N_{dist}^{obs} = 1. \quad (16)$$

485

486 The first relation holds when none of the distributaries discharge more sediment
487 than Q_{wave}, otherwise mouthbars would have been formed and N_{dist}^{obs} would have been
488 higher. On the other hand, for deltas with single-threaded channels ($N_{dist}^{obs} = 1$) and
489 smooth shorelines, we measured the delta flanks angles relative to a reference shoreline
490 to quantify the observed wave flux, $Q_{w,net}^{obs}$ (Figure 4D). In Eq. 16, θ_{right}^{obs} and θ_{left}^{obs} are the
491 observed right and left delta flank angles with respect to the reference shoreline
492 orientation, and $Q_{w,net}(\theta)$ is the observed net alongshore sediment transport for an
493 observed angle θ.

494 As in the predictions, the protrusion angle is the average of flank angles that
495 represents how far or close the delta is from the maximum wave transport capacity,
496 reaching the maximum for a protrusion angle of ~45°. These angles give an alongshore
497 transport left of the river mouth as $Q_{w,net}$ for $0 < \theta < \frac{\pi}{2}$, and transport right of the river
498 mouth as $Q_{w,net}$ for $-\frac{\pi}{2} < \theta < 0$. The difference in transport between the left and right
499 flank of the delta should, at equilibrium, be equal to the fluvial sediment flux Q_{river}. Its
500 comparison with the predicted potential maximum wave flux (Q_{wave}, Eq. 4) then gives an
501 indication of the observed river-dominance ratio R^{obs} (Eq. 16).

502

503 ***3.2.2. Observed Tide Dominance***

504 Like the relation of shoreline shape to river-dominance ratio, we can recast the
505 observed channel widening into an observed tide-dominance ratio (T^{obs}) as (Nienhuis et
506 al., 2018, their Eq. 8)

507

$$T^{obs} = \left(\frac{w_m}{w_u}\right|^{obs} - 1\Big) Uf, \quad 17$$

508

509 where w_m is a single mouth width ($w_m = \Sigma_n w_{m,n}/N_{dist}^{0.5}$ for multiple distributaries),
510 w_u is the fluvial channel width, $U = \frac{0.5\omega a}{S \cdot u_{river}}$ is the strength of the tidal flow relative to the
511 fluvial flow (with tidal quantities given above), $f = 1 + \frac{2S}{ka}$ as given above. Tidal quantities
512 (ω and a) are determined for the constituent (i.e., M_2, S_2, N_2, K_1, or O_1) with the largest
513 amplitude a, which corresponds to the long-term average tidal amplitude. Fluvial flow is
514 represented by $u_{river} = Q_{w,River}\beta/w_u^2$, with $\beta = \frac{w_u}{d}$, $d = 0.6 \cdot Q_{w,river}^{1/3}$ (Mikhailov, 1970, Eq.
515 21). Note that $Q_{w,River}$ is the fluvial discharge, contrary to the sediment load given by
516 Q_{river}.

517 ***3.2.3. Observations in the ternary space***

518 We place the observed morphology into ternary space to ease visualization and
519 allow for a non-dimensional comparison with predictions across morphologic thresholds
520 (cf. observed angle vs. predicted shoreline angles). To do this, we use the observed fluvial
521 sediment flux Q_{river}, and derive Q_{tide}^{obs}, and Q_{wave}^{obs}. We quantify the tidal sediment flux
522 based on T^{obs}, as in $Q_{tide}^{obs} = T^{obs} \cdot Q_{river}$. We formulate an observed wave sediment flux
523 Q_{wave}^{obs} from R^{obs}, using $Q_{wave}^{obs} = \frac{Q_{river}}{R^{obs}}$. We then determine the relative fluxes within the
524 ternary diagram by calculating r_x^{obs} (Eq. 1).

525

526 **3.3. Predictions versus Observations**

527 To assess our predictions accuracy, we calculated a ternary error, e_{ter}, as the
528 Euclidian distance within the ternary diagram between the observed and predicted
529 locations as

530

$$e_{ter} = \sqrt{\left[\tfrac{1}{2}\left(r_{river}^{pred} - r_{river}^{obs}\right) + \left(r_{tide}^{pred} - r_{tide}^{obs}\right)\right]^2 + \tfrac{3}{4}\left[r_{river}^{pred} - r_{river}^{obs}\right]^2}, \quad 18$$

531

532 which is based on to the cartesian coordinates within the triangle, x and y, and
533 their relation to ternary coordinates, r_x, as $y = r_{river} \sin 60° = \sqrt{3} r_{river}/2$ and $x = r_{tide} +$
534 $y \cot 60° = r_{tide} + r_{river}/2$. e_{ter} is 0 for accurate predictions and 1 for predictions that
535 render a fully opposite dominance (e.g., $r_{river}^{pred} = 1$ but $r_{river}^{obs} = 0$, Figure 6).

536

4. Results

4.1. Prediction of Delta Morphology

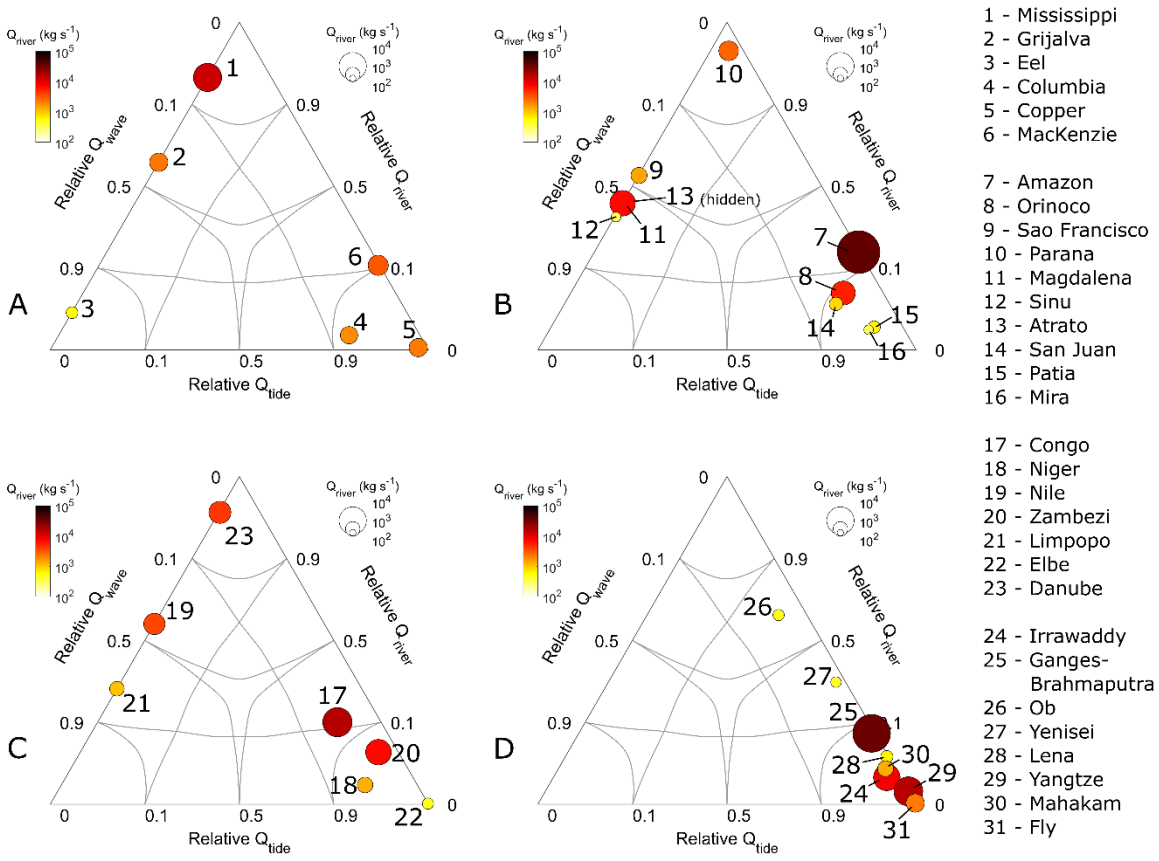

Figure 7. Ternary diagrams with the prediction of delta morphology for our 31 deltas. We organized deltas in continents as (A) North America, (B) South America, (C) Africa and Europe, and (D) Asia and Oceania. See Figure 1 and for locations. Axes are in sigmoid scaling to help distinguish extreme values.

From our selection of deltas, we predict ~23% to be fluvial-dominated (7 out of 31 deltas), ~16% wave-dominated (5 out of 31), and ~61% tide-dominated (19 out of 31), with broad representation all across the ternary space (Figure 7). However, the degree of dominance we predicted vary among deltas, as demonstrated by the number of distributaries (55.9±127.5, 1 standard deviation), shoreline protrusion angle (14.1°±12°, 1 std, with 20 out of 31 deltas with undefined (river-dominated) protrusion), and channel widening (53.5±170.8, 1 std).

We predict fluvial dominance for the Mississippi ($r_{River} = 0.95$, 20 distributaries) and wave dominance for the Eel ($r_{Wave} = 0.97$, cuspate angle of 0.8°). We predict tidal dominance for the Copper ($r_{Tide} \approx 1.0$ and channel widening of 856.3), and fluvial dominance for the Parana ($r_{River} = 0.99$ with 172 distributaries). Some deltas have a predicted mixed influence, such as the Atrato ($r_{River} = 0.59$ with 2 distributaries, $r_{Wave} = 0.41$) and the Nile ($r_{River} = 0.64$ with 2 distributaries).

4.2. Delta Morphology Observations

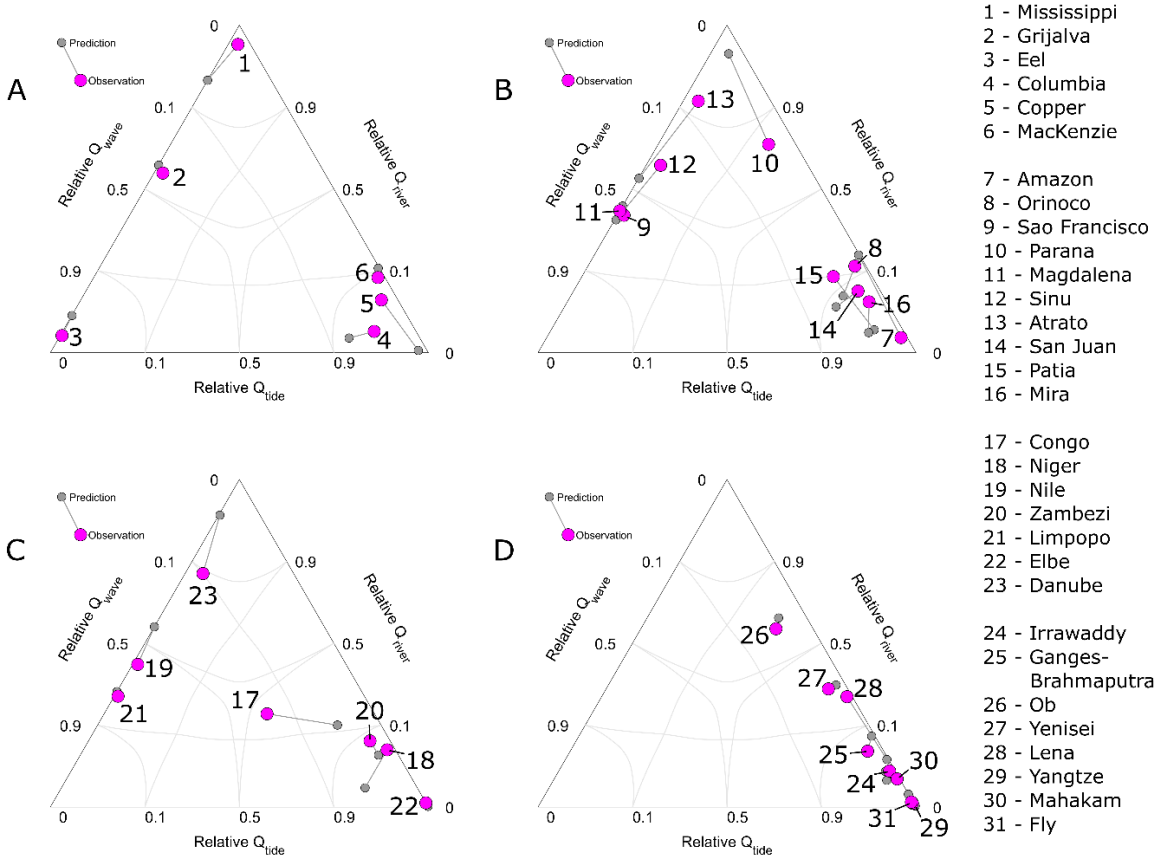

Figure 8. Ternary diagrams from observation-based fluxes of delta morphology for the 31 deltas (magenta dots) compared to predictions in Figure 7 (gray dots). (A) North America, (B) South America, (C) Africa and Europe, and (D) Asia and Oceania. Axes are in sigmoid scaling to distinguish among extreme values.

In our morphological observations, we find 23% to be fluvial-dominated (7 out of 31 deltas), 16% wave-dominated (5 out of 31), and 61% tide-dominated (19 out of 31). The skew toward tide-dominance compared to global deltas broadly (Nienhuis et al., 20202) is likely because of our selection of mostly larger deltas. We observe fluvial dominance for the Mississippi ($r_{River}^{obs} = 0.99$, 219 distributaries) and Atrato ($r_{River}^{obs} 0.93$ with 14 distributaries). Other deltas, such as the Sao Francisco ($r_{Wave}^{obs} = 0.70$ with protrusion angle 19.8°) and the Magdalena ($r_{Wave}^{obs} = 0.68$ with protrusion angle 30.8°) are observed as wave dominated.

4.3. Predictions versus Observations

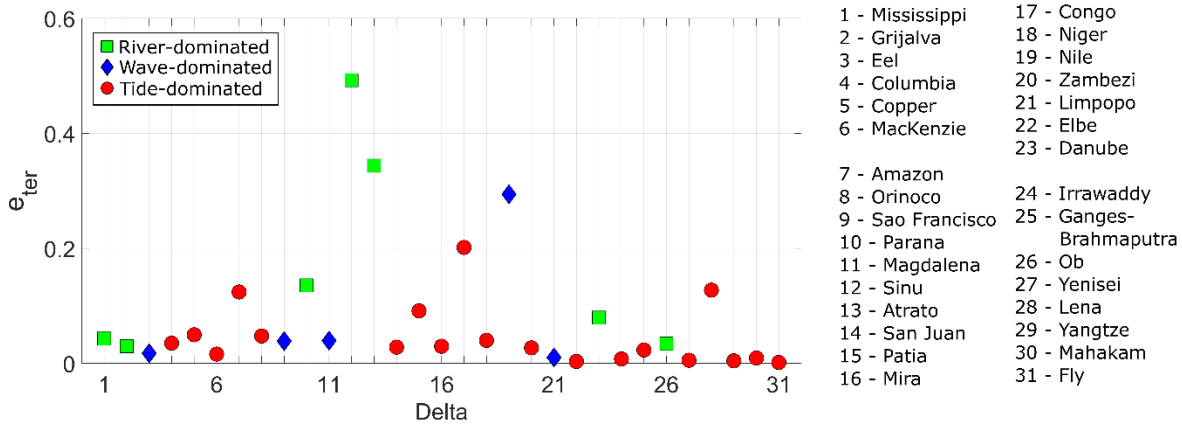

Figure 9. Ternary error in predictions, e_{ter}, with observed dominance indicated by symbols (fluvial: green squares, wave: blue diamonds, tide: red circles).

Comparing predictions and observations, we find that errors (e_{ter}) are typically <0.20 (28 out of 31 deltas), with a maximum of ~0.49 (Sinu delta), minimum of 0.002 (Fly delta) (Figure 9). The mean error is 0.08 ± 0.11 (1 std). From the 3 deltas with $e_{ter} > 0.20$, the largest errors correspond to river-dominated deltas. Overall, tide-dominated deltas exhibit errors <0.20 (all 19 deltas), with 15 deltas with errors <0.05. However, other fluvial- and wave-dominated deltas also exhibit errors close to 0 (e.g., Eel, Limpopo, and Ob). Categorically, we find that 29 out of the 31 deltas are classified correctly (e.g., predicted and observed as wave-dominated).

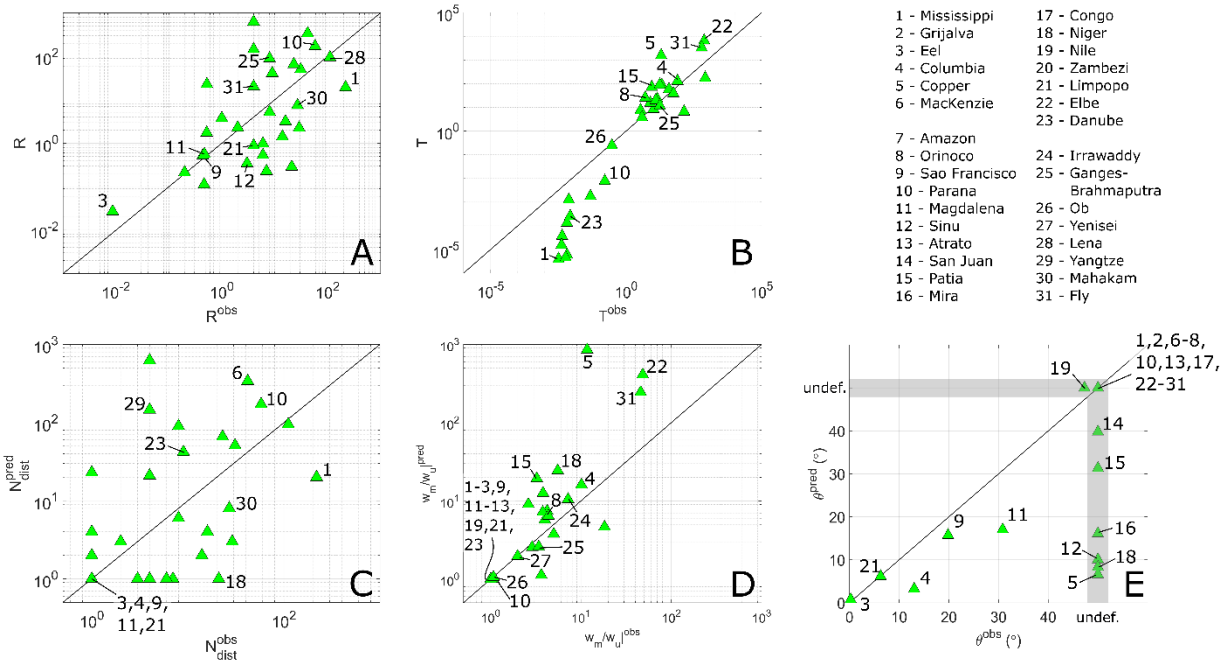

Figure 10. Comparison of morphology predictions and observations for the 31 deltas. (A) Fluvial dominance factor. (B) Tide dominance factor. (C) Number of distributaries. (D) Downstream channel widening. (E) Protrusion angle.

We find that there is no strong bias in our predictions for the fluvial dominance ratio, although there is scatter ($R^{obs} < R$ for 16 deltas, and $R^{obs} > R$ for 15 deltas). Tidal dominance tends to be underpredicted for wave and river-dominated deltas ($T^{obs} < 1$) and overpredicted for tide-dominated deltas (Figure 10B). This is likely due to underprediction of Q_{tide} (see below for sources of uncertainty) that rendered $T < T^{obs}$ for fluvially-dominated deltas (e.g., Mississippi, Danube, Parana) with $T^{obs} < 1$.

Individual morphological error metrics show greater variability (Figure 10C-E). We overpredicted the number of distributaries for 13 deltas, including 6 deltas with 1 predicted and observed distributary (Figure 10C). We overpredicted the channel widening for 13 deltas and predicted and observed no widening (=1) for 12 deltas (Figure 10D). We overpredicted the protrusion angles for 2 deltas and found 18 with undefined predicted and observed angles (Figure 10E).

5. Discussion

This work compares delta morphology predictions and observations for 31 selected deltas, using a novel methodology that expands on the quantitative Galloway ternary diagram. In general, our predictions follow closely the observations, with $e_{ter} = 0.08 \pm 0.21$. We found that most of our tide-dominated deltas exhibited the smallest error, although errors for wave and river dominated deltas were also close to zero, with a maximum error of 0.49. We now analyze some examples of morphology prediction and observation, including sources of uncertainty and effects of human interventions.

5.1. Source of Uncertainty

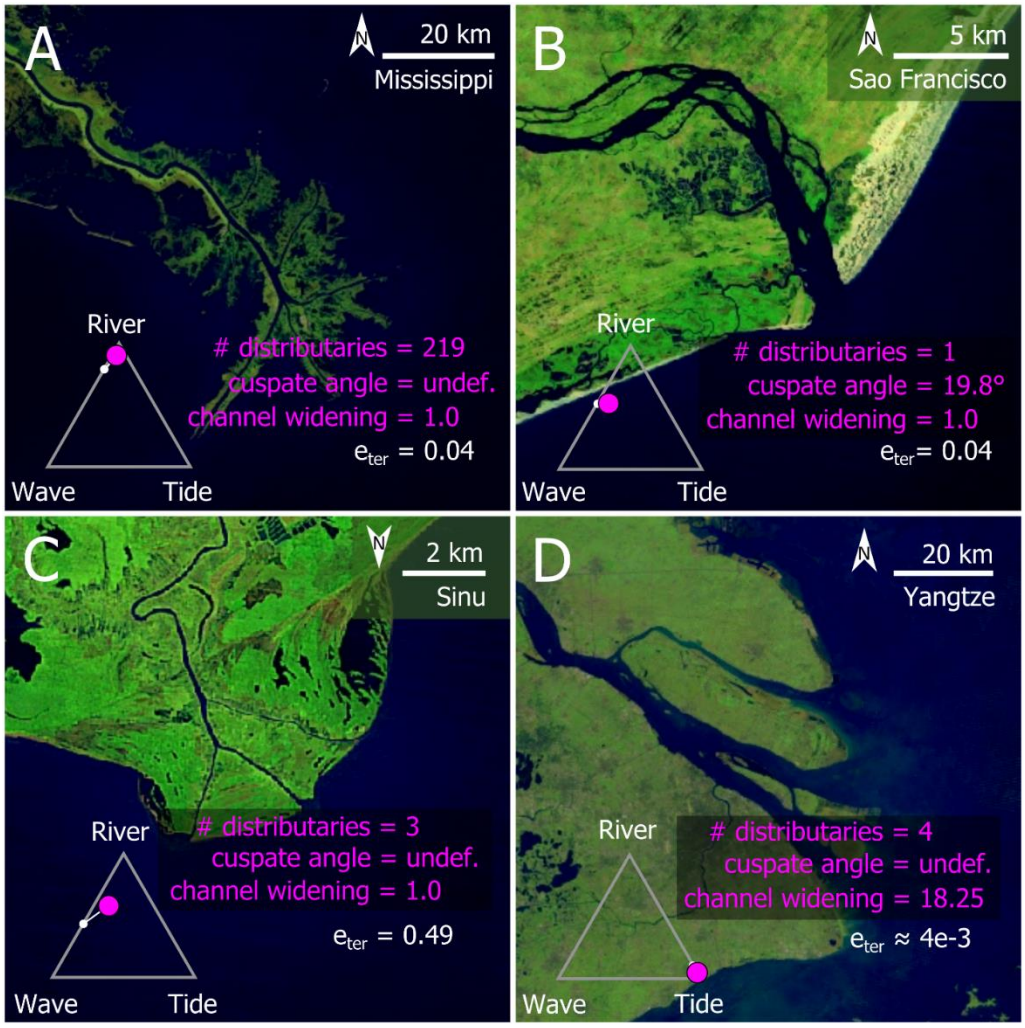

Figure 11. Examples delta morphology prediction (white dot) and observation (magenta dot) within the ternary diagram, including observed morphology and ternary error, e_{ter}. (A) Mississippi, (B) Sao Francisco, (C) Sinu, and (D) Yangtze. Imagery from Aquamonitor (https://aqua-monitor.appspot.com/).

The ternary errors between observations and predictions have their origin in different sources. Morphological observations are uncertain and include measurement error. Predictions are based on data and models providing ocean and terrestrial conditions (wave heights, tidal amplitude, river sediment discharge), in addition to assumptions on processes shaping delta morphology. There are also elements of time and spatial scales that are challenging to resolve and result in an uncertainty. Predictions are based on the sediment fluxes at the delta apex, and averaged over the past ~30 years, even though dominant morphological processes vary spatially within a delta (Broaddus et al., 2022) and vary in time.

Table 1. Errors in predictions and sources of uncertainty for 4 selected deltas in Figure 11.

Delta		e_{ter}	Observed dominance	Prediction/observation comparison - fluxes prediction	Most prominent potential source of error	Particularities
1	Mississippi	0.043	River	Predicted less distributary mouths - overprediction of wave fluxes	Theoretical - assumption of maximum wave transport capacity at each mouth of multi-channel deltas	Channel diversions, levees, large subsidence (Törnqvist et al., 2008; Xu et al., 2019; Zhang et al., 2022)
9	Sao Francisco	0.039	Wave	Predicted more distributary mouths and larger cuspate angle - underprediction of wave fluxes	Theoretical - wind-wave dissipation and scattering over continental shelves	Strandplain with inactive and active dune fields (Barbosa & Dominguez, 2004; Dominguez, 1996)
12	Sinu	0.493	River	Predicted less distributary mouths and smaller cuspate angle - overprediction of wave fluxes	Theoretical - wind-wave dissipation and scattering over continental shelves	Muddy coast, upstream water diversions (Piccardi et al., 2020; Serrano Suarez, 2004)

29	Yangtze	0.004	Tide	Predicted more distributary mouths and smaller channel widening - underprediction of wave and tidal fluxes	Theoretical - wind-wave dissipation and scattering over continental shelves	Upstream basin degradation, delta land reclamation, shoreline embamkment (Saito et al., 2001; Wang et al., 2011; Zhang et al., 2022)

Various sources of error are difficult to disentangle. Here we explored potential sources of uncertainty by comparing predicted and observed morphological features, i.e., number of distributary mouths, cuspate angle, and channel widening (Table 1). We can use this comparison to identify what explains the prediction errors, i.e., either over- or underpredicting wave, river, or tidal fluxes (or a combination of them).

For the Mississippi (Figure 11A), we underpredicted the distributary mouths (20 predicted, 219 observed), which we relate to an overprediction of wave fluxes. This error relates to our theoretical assumption of maximum wave flux capacity at each mouth, whereas most mouths will be sheltered from the dominant ocean waves and can more easily build mouthbars (Edmonds & Slingerland, 2010). The fluvial sediment flux can also be underpredicted.

For the Sao Francisco (Figure 11B), we found similar cuspate angles (15.7° predicted, 19.8° observed). We relate the difference to an overprediction of wave fluxes that render a smaller predicted angle. For the Sinu delta (Figure 11C), we predict a relatively small cuspate angle (10.1°) versus our observation of 3 distributary mouths, which we relate to an overprediction of wave fluxes. For the Yangtze (Figure 11D), we overpredict the number of distributaries (146 predicted, 4 observed) and underpredict the channel widening (4.66 predicted, 18.25 observed). We relate these errors to an underprediction of wave and tidal fluxes.

We can explain the underprediction of wind waves and tides by considering nonlinear transformations over complicated bathymetry that our theory didn't capture. It is known that waves can increase their energy flux onshore of complicated bathymetry, i.e., sand shoals, canyons, etc. (Bender & Dean, 2005; Bing Wang et al., 2014; Eslami et al., 2019; Paniagua-Arroyave et al., 2019). Conversely, fine sediment dynamics can decrease shoreline wave energy fluxes and tidal amplitudes (Elgar & Raubenheimer,

2008; Winterwerp et al., 2007). These phenomena likely influence the difference between predictions and observations as we over- or under-predict wave energy fluxes, hence sediment transport by waves and tides. Our theory also assumes that, for multiple distributary mouths, each mouth would carry the same amount of fluvial sediment, which does not reflect nature (Bolla Pittaluga et al., 2015). Therefore, we assume that waves can move the maximum capacity at each mouth, which can overestimate the total sediment flux at the delta.

5.2. Uncertainties and Limitations

5.2.1. Human Interventions

Part of the uncertainty in morphological predictions stem from the effects of human interference (Zhang et al., 2022). This is a broad topic; therefore, we discuss this using the Magdalena River delta at Bocas de Ceniza (delta 11) as case study. The Magdalena delta (Figure 12) is located on the threshold between fluvial and wave dominance. We observe one distributary mouth, a cuspate angle of 30.8° and channel widening of 1 ($R^{obs} = 0.47$, $T^{obs} = 0$). The ternary error is ~0.04. Our observations are very similar to the predictions, i.e., 1 distributary, cuspate angle of 17°, and channel widening of 1 ($R = 0.56$, $T = 0$) (Figure 12A). At first, our method is successful in prognosing this delta. However, modern delta morphology is controlled by engineering structures that stabilize the mouth channel width and influence morphodynamics (Figure 12B).

Historical maps from 1843 (Martinez et al., 1990) show a single distributary mouth with alongshore extending spits and a general westward orientation (Figure 12C). This morphology suggests wave dominance with a shoreline deflection that indicates sediment bypassing and wave climate control (Nienhuis et al., 2016). Note that the historical Magdalena is similar to our predictions (1 distributary, 17° of cuspate angle, no channel widening).

We argue that our observations capture wave flank angles and a single distributary mouth that are unbalanced. The observed Magdalena delta flanks have angles that might maximize wave fluxes locally, but don't maximize the overall wave flux at the mouth. The measured angles, i.e., 31.3° (left) and –30.4° (right), differ from the flank angles that maximize wave fluxes, i.e., 90° (left) and 19° (right), both positive. This morphology that

maximizes Q_{Wave} would resemble the modern Buritaca delta in Colombia and the historical Magdalena delta morphology (Martinez et al., 1990). The unbalanced morphology relies on human structures that concentrate the flow, preventing sediment bypassing and shoreline deflection. We speculate that a surplus of sediment gets routed to a nearby submarine canyon given that the delta flanks are fixed by jetties and waves cannot effectively modify the morphology (e.g., Naranjo-Vesga et al., 2021).

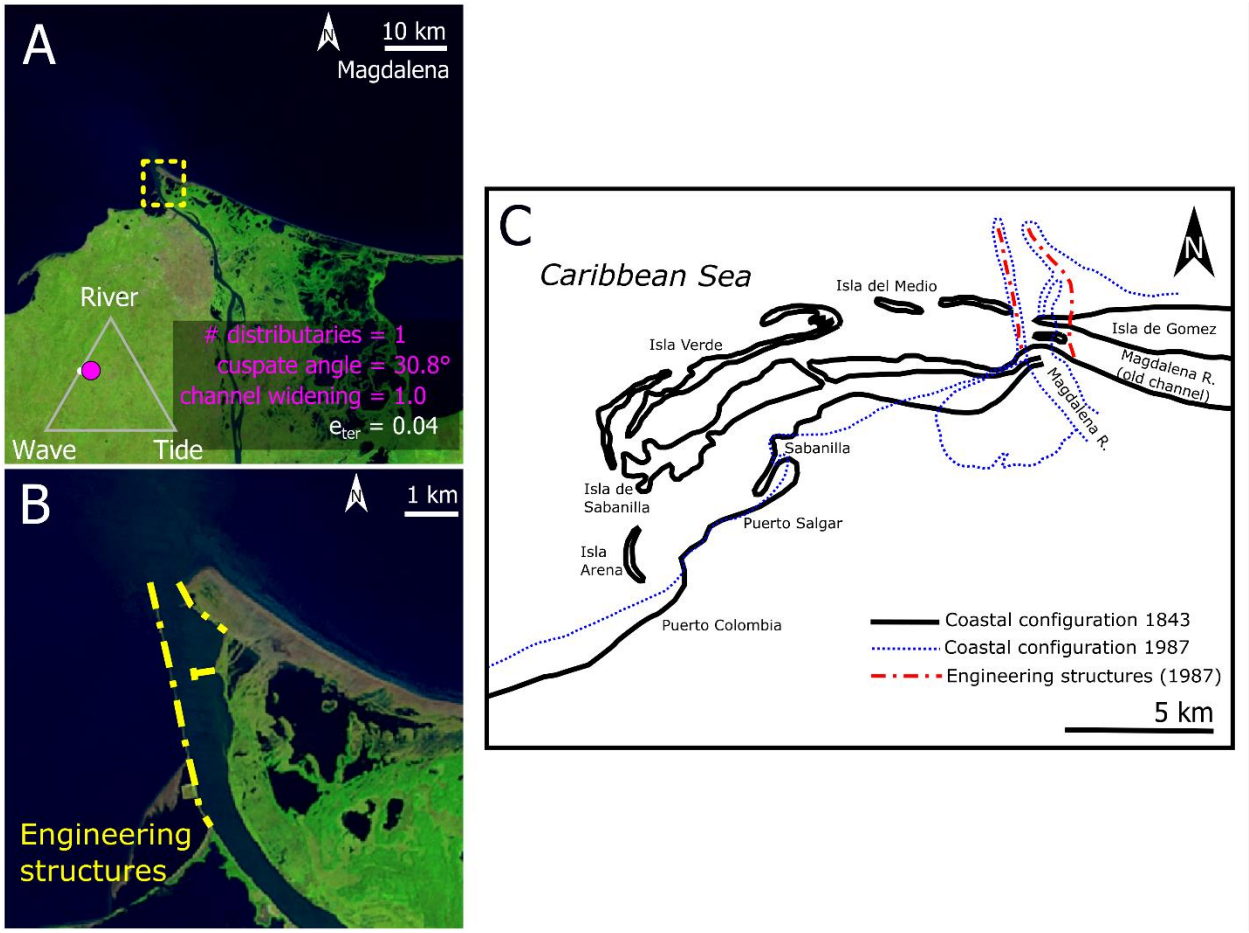

Figure 12. Example of effects of engineering in delta morphology and its representation in the Galloway diagram. (A) Magdalena delta at Bocas de Ceniza (near Barranquilla city) in 2022, with yellow box showing the location of close up in panel B. (B) Close up to the Magdalena River mouth, showing current engineering structures at mouth flanks (yellow lines). (C) Historical delta morphology (1843 and 1987). Modified from Martínez et al. (1990, their Fig. 2).

5.2.2. Limitations

First, we stress that we do not focus on the observed fluxes. Instead, we use the relative fluxes to infer dominance and compare predictions and observations. Our observed fluxes are extreme in several cases (e.g., $Q_{Tide}^{obs} \approx 5.2 \times 10^6\ kg/s$ for the Amazon, $Q_{Tide}^{obs} \approx 12.2 \times 10^6\ kg/s$ for the Yangtze, or $Q_{Wave}^{obs} \approx 14{,}834\ kg/s$ for the Magdalena). These values highlight the relative nature of our observed fluxes. We include them for clarity in the methodology and it could be argued that they can represent sediment retention to a certain point. However, the retention argument is beyond the scope of the present manuscript and these values should be considered artifacts of our theoretical approach instead of actual observations.

We further acknowledge three sources of error for our results: (1) data for predictions, (2) morphological observations, and (3) theoretical models. In the case of data, riverine fluxes from WBMSed v2 (Cohen et al., 2014) include an average error of ~34%. The inclusion of this error could be problematic when cataloging deltas according to their mixed dominance, e.g., when a delta exhibits tide-river or wave-river dominance. This error affects both predictions and observations since we use Q_{river} for both calculations. Also, errors from the wave (WaveWatch III, Chawla et al., 2013) and tidal (TPX, Egbert & Erofeeva, 2002) models could be considered negligible, although wave transformation over continental shelves for both wind-waves and tides in our methods is crude and requires improvement, especially along complicated coastlines (canyons, muddy coastlines, etc.).

Second, errors in our morphological observations (number of distributary channels, upstream and mouth channel widths, channel slopes, and flank angles) depend upon the digitizer criteria and precision and are typically in the order of centimeters according to pixel sizes of the latest Google Earth imagery. Measuring channel slope for tidal fluxes quantification includes a significant error because of the crude topographic data from the 1 arc-sec SRTM. Morphology errors might also be related to omitting distributaries, not process-based locations to measure the upstream or mouth channel widths, and arbitrary digitizing the general shoreline in complicated wave-dominated deltas (e.g., Magdalena).

728 Finally, a fundamental error lies in our theoretical models, both for predictions and
729 observations. Despite we applied a powerful approach to analyze sediment balance at
730 wave-dominated deltas (Nienhuis et al., 2015, 2016), the formalism of sediment transport
731 by waves (Ashton & Murray, 2006) has shortcomings when compared to field
732 observations (Cooper & Pilkey, 2004). Also, our approach to assessing tidal dominance
733 proves to render good results here and elsewhere (Nienhuis et al., 2018). However, it
734 simplifies the actual tidal hydrodynamics that controls sediment transport and land
735 building, especially for deltas with multiple distributaries (e.g., Hoitink & Jay, 2016).

736

6. Conclusions

We propose a novel method to compare river delta morphology predictions with observations. It expands beyond earlier work that predicts delta morphology from the balance of fluvial, tidal, and wave sediment fluxes, and allows us to compare different sources of morphological uncertainties in a non-dimensional framework. The application of our method to a selection of 31 deltas globally rendered a ternary error of 8% (±11%, 1 standard deviation), with no strong bias toward one of the three dominant morphologies. Relative uncertainties in predictions of shoreline angle (14.1°±12° predicted vs. 20.8°±16.1° observed), downstream widening of delta channels (53.5±170.8 predicted vs. 6.5±11.5 observed), and number of distributary channels (55.9±127.5 predicted vs. 21.4±43.0 observed) are similar. We estimate that the inaccurate calculation of wave and tidal fluxes is the largest source of uncertainty for delta morphology predictions, compared to fluvial sediment supply. As our approach predicts first-order delta morphology from sediment fluxes, it offers a way of forecasting how delta morphology will adjust to variations in sediment flux balances, with potential applications to deltas worldwide under climate and global change stressors.

Acknowledgments

This research was supported by the U. S. National Science Foundation (award EAR-1810855 to JHN); and the Vice-President Office for Science, Technology, and Innovation at EAFIT University (award 952-000015 to JFPA). We thank J.D. Restrepo-Ángel, A. Valle-Levinson, A.J.F. Hoitink, Y. Saito, L. Velasquez-Montoya, O. Álvarez-Silva, E. Ramos-Chavarriaga, A. Amaya-Saldarriaga, J. Vargas-Londoño, J.L. Restrepo-Muñoz, and D.A. Arboleda-Girón for thoughtful discussions that enriched this research. Data and supplementary codes can be found at http://dx.doi.org/10.17632/j83n7hbvst.1.

References

Ashton, A. D., & Giosan, L. (2011). Wave-angle control of delta evolution. *Geophysical Research Letters*, *38*(13), 1–6. https://doi.org/10.1029/2011GL047630

Ashton, A. D., & Murray, A. B. (2006). High-angle wave instability and emergent shoreline shapes: 1. Modeling of sand waves, flying spits, and capes. *Journal of Geophysical Research: Earth Surface*, *111*(4), 1–19. https://doi.org/10.1029/2005JF000422

Barbosa, L. M., & Dominguez, J. M. L. (2004). Coastal dune fields at the São Francisco River strandplain, northeastern Brazil: Morphology and environmental controls. *Earth Surface Processes and Landforms*, *29*(4), 443–456. https://doi.org/10.1002/ESP.1040

Baumgardner, S. E. (2016). *Quantifying Galloway: Fluvial, Tidal and Wave Influence on Experimental and Field Deltas* (Doctoral dissertation). University of Minnesota.

Bender, C. J., & Dean, R. G. (2005). Wave transformation by axisymmetric three-dimensional bathymetric anomalies with gradual transitions in depth. *Coastal Engineering*, *52*(4), 331–351. https://doi.org/10.1016/j.coastaleng.2004.12.005

Bentley, S. J., Blum, M. D., Maloney, J., Pond, L., & Paulsell, R. (2016). The Mississippi River source-to-sink system: Perspectives on tectonic, climatic, and anthropogenic influences, Miocene to Anthropocene. *Earth-Science Reviews*, *153*, 139–174. https://doi.org/10.1016/j.earscirev.2015.11.001

Best, J. (2019). Anthropogenic stresses on the world's big rivers. *Nature Geoscience*, *12*(1), 7–21. https://doi.org/10.1038/s41561-018-0262-x

Bing Wang, Z., Winterwerp, J. C., & He, Q. (2014). Interaction between suspended sediment and tidal amplification in the Guadalquivir Estuary. *Ocean Dynamics*, *64*, 1487–1498. https://doi.org/10.1007/s10236-014-0758-x

Bolla Pittaluga, M., Coco, G., & Kleinhans, M. G. (2015). A unified framework for stability of channel bifurcations in gravel and sand fluvial systems. *Geophysical Research Letters*, *42*(18), 7521–7536. https://doi.org/10.1002/2015GL065175

Boyd, R., Dalrymple, R., & Zaitlin, B. A. (1992). Classification of clastic coastal depositional environments. *Sedimentary Geology*, *80*(3–4), 139–150. https://doi.org/10.1016/0037-0738(92)90037-R

Broaddus, C. M., Vulis, L. M., Nienhuis, J. H., Tejedor, A., Brown, J., Foufoula-Georgiou, E., & Edmonds, D. A. (2022). First-order River Delta Morphology is Explained by the Sediment Flux Balance from Rivers, Waves, and Tides. *Geophysical Research Letters*. https://doi.org/10.1029/2022gl100355

Chawla, A., Spindler, D. M., & Tolman, H. L. (2013). Validation of a thirty year wave hindcast using the Climate Forecast System Reanalysis winds. *Ocean Modelling*, *70*, 189–206. https://doi.org/10.1016/j.ocemod.2012.07.005

Coffey, T. S., & Shaw, J. B. (2017). Congruent Bifurcation Angles in River Delta and Tributary Channel Networks. *Geophysical Research Letters*, *44*(22), 11,427-11,436. https://doi.org/10.1002/2017GL074873

Cohen, S., Kettner, A. J., & Syvitski, J. P. M. (2014). Global suspended sediment and water discharge dynamics between 1960 and 2010: Continental trends and intra-basin sensitivity. *Global and Planetary Change*, *115*, 44–58. https://doi.org/10.1016/j.gloplacha.2014.01.011

Coleman, J. M., & Wright, L. D. (1975). Modern River Deltas: Variability of Processes and Sand Bodies. In M. lou Broussard (Ed.), *Deltas, Models for Exploration* (pp. 99–150). Houston, TX, USA: Houston Geological Society.

Cooper, J. A. G., & Pilkey, O. H. (2004). Longshore drift: Trapped in an expected universe. *Journal of Sedimentary Research*, *74*(5), 599–606. https://doi.org/10.1306/022204740599

Dalrymple, R. W., Zaitlin, B. A., & Boyd, R. (1992). Estuarine facies models : conceptual basis and stratigraphic implications. *Journal of Sedimentary Petrology*, *62*(6), 1130–1146. https://doi.org/10.1306/D4267A69-2B26-11D7-8648000102C1865D

Dan, S., Walstra, D. J. R., Stive, M. J. F., & Panin, N. (2011). Processes controlling the development of a river mouth spit. *Marine Geology*, *280*(1–4), 116–129. https://doi.org/10.1016/j.margeo.2010.12.005

Dominguez, J. M. L. (1996). The Sao Francisco strandplain: a paradigm for wave-dominated deltas? In M. de Batist & P. Jacobs (Eds.), *Geology of Siliciclastic Shelf Seas* (pp. 217–231). Geological Society Special Publication No. 117. Retrieved from https://www.lyellcollection.org

Donchyts, G., Baart, F., Winsemius, H., Gorelick, N., Kwadijk, J., & van de Giesen, N. (2016). Earth's surface water change over the past 30 years. *Nature Climate Change*, *6*(9), 810–813. https://doi.org/10.1038/nclimate3111

Edmonds, D. A., & Slingerland, R. L. (2010). Significant effect of sediment cohesion on deltamorphology. *Nature Geoscience*, *3*(2), 105–109. https://doi.org/10.1038/ngeo730

Egbert, G. D., & Erofeeva, S. Y. (2002). Efficient inverse modeling of barotropic ocean tides. *Journal of Atmospheric and Oceanic Technology*, *19*(2), 183–204. https://doi.org/10.1175/1520-0426(2002)019<0183:EIMOBO>2.0.CO;2

Elgar, S., & Raubenheimer, B. (2008). Wave dissipation by muddy seafloors. *Geophysical Research Letters*, *35*(7). https://doi.org/10.1029/2008GL033245

Eslami, S., Hoekstra, P., Nguyen Trung, N., Ahmed Kantoush, S., van Binh, D., Duc Dung, D., et al. (2019). Tidal amplification and salt intrusion in the Mekong Delta driven by anthropogenic sediment starvation. *Scientific Reports 2019 9:1*, *9*(1), 1–10. https://doi.org/10.1038/s41598-019-55018-9

Fagherazzi, S., & Overeem, I. (2007). Models of Deltaic and Inner Continental Shelf Landform Evolution. *Annual Reviews of Earth and Planetary Science*, *35*, 685–715. Retrieved from https://www.annualreviews.org/doi/full/10.1146/annurev.earth.35.031306.140128#article-denial

Galloway, W. E. (1975). Process Framework for Describing the Morphologic and Stratigraphic Evolution of Deltaic Depositional Systems. In M. lou Broussard (Ed.), *Deltas, Models for Exploration*. Houston, TX, USA: Houston Geological Society.

Gao, S., Wang, Y. P., & Gao, J. hua. (2011). Sediment retention at the Changjiang sub-aqueous delta over a 57 year period, in response to catchment changes. *Estuarine, Coastal and Shelf Science*, *95*(1), 29–38. https://doi.org/10.1016/j.ecss.2011.07.015

Gilbert, G. K. (1885). *The topographic features of lake shores*. Washington DC, USA.

Goodbred, S. L., & Saito, Y. (2012). Tide-Dominated Deltas. In R. A. Davis & R. W. Dalrymple (Eds.), *Principles of Tidal Sedimentology* (pp. 129–149). Dordrecht, The Netherlands: Springer.

Hoitink, A. J. F., & Jay, D. A. (2016). Tidal river dynamics: Implications for deltas. *Reviews of Geophysics*, *54*(1), 240–272. https://doi.org/10.1002/2015RG000507

Hoitink, A. J. F., Nittrouer, J. A., Passalacqua, P., Shaw, J. B., Langendoen, E. J., Huismans, Y., & van Maren, D. S. (2020). Resilience of River Deltas in the Anthropocene. *Journal of Geophysical Research: Earth Surface*, *125*(3), 1–24. https://doi.org/10.1029/2019JF005201

Jerolmack, D. J., & Swenson, J. B. (2007). Scaling relationships and evolution of distributary networks on wave-influenced deltas. *Geophysical Research Letters*, *34*(23). https://doi.org/10.1029/2007GL031823

Jobe, Z. R., Sylvester, Z., Parker, A. O., Howes, N., Slowey, N., & Pirmez, C. (2015). Rapid adjustment of submarine channel architecture to changes in sediment supply. *Journal of Sedimentary Research*, *85*(6), 729–756. https://doi.org/10.2110/jsr.2015.30

Ke, W. T., Shaw, J. B., Mahon, R. C., & Cathcart, C. A. (2019). Distributary Channel Networks as Moving Boundaries: Causes and Morphodynamic Effects. *Journal of Geophysical Research: Earth Surface*, *124*(7), 1878–1898. https://doi.org/10.1029/2019JF005084

Komar, P. D. (1973). Computer Models of Delta Growth due to Sediment Input from Rivers and Longshore Transport. *Geological Society of America Bulletin*, *84*, 2217–2226.

Konkol, A., Schwenk, J., Katifori, E., & Shaw, J. B. (2022). Interplay of River and Tidal Forcings Promotes Loops in Coastal Channel Networks. *Geophysical Research Letters*, *49*(10). https://doi.org/10.1029/2022GL098284

Liu, J. P., Xue, Z., Ross, K., Wang, H. J., Yang, Z. S., Li, A. C., & Gao, S. (2009). Fate of sediments delivered to the sea by Asian large rivers: Long-distance transport and formation of remote alongshore clinothems. *The Sedimentary Record*, *7*(4), 4–9.

Martinez, J. O., Pilkey, O. H., & Neal, W. J. (1990). Rapid formation of large coastal sand bodies after emplacement of Magdalena river jetties, northern Colombia. *Environmental Geology and Water Sciences*, *16*(3), 187–194. https://doi.org/10.1007/BF01706043

Mikhailov, V. N. (1970). Hydrologic-morphometric characteristics of delta branches. *Stud. Rep. Hydrol.*, *9*, 146–158. Retrieved from http://iahs.info/redbooks/a090/iahs_090_0146.pdf

Naranjo-Vesga, J., Ortiz-Karpf, A., Wood, L., Jobe, Z., Paniagua-Arroyave, J. F., Shumaker, L., et al. (2020). Regional controls in the distribution and morphometry of deep-water gravitational deposits along a convergent tectonic margin. Southern caribbean of Colombia. *Marine and Petroleum Geology*, *121*(April), 104639. https://doi.org/10.1016/j.marpetgeo.2020.104639

Naranjo-Vesga, J., Paniagua-Arroyave, J. F., Ortiz-Karpf, A., Wood, L., Jobe, Z., Galindo, P., et al. (2021). Controls on submarine canyon morphology along a convergent tectonic margin. The Southern Caribbean of Colombia. *Marine and Petroleum Geology*, *105493*. https://doi.org/10.1016/j.marpetgeo.2021.105493

Nienhuis, J. H., & van de Wal, R. S. W. (2021). Projections of Global Delta Land Loss From Sea-Level Rise in the 21st Century. *Geophysical Research Letters*, *48*(14), 1–9. https://doi.org/10.1029/2021GL093368

Nienhuis, J. H., Ashton, A. D., & Giosan, L. (2015). What makes a delta wave-dominated? *Geology*, *43*(6), 511–514. https://doi.org/10.1130/G36518.1

Nienhuis, J. H., Ashton, A. D., Nardin, W., Fagherazzi, S., & Giosan, L. (2016). Alongshore sediment bypassing as a control on river mouth morphodynamics. *Journal of Geophysical Research F: Earth Surface*, *121*(4), 664–683. https://doi.org/10.1002/2015JF003780

Nienhuis, J. H., Hoitink, A. J. F. T., & Törnqvist, T. E. (2018). Future Change to Tide-Influenced Deltas. *Geophysical Research Letters*, *45*(8), 3499–3507. https://doi.org/10.1029/2018GL077638

Nienhuis, J. H., Ashton, A. D., Edmonds, D. A., Hoitink, A. J. F., Kettner, A. J., Rowland, J. C., & Törnqvist, T. E. (2020). Global-scale human impact on delta morphology has led to net land area gain. *Nature*, *577*(7791), 514–518. https://doi.org/10.1038/s41586-019-1905-9

Nienhuis, J. H., Kim, W., Milne, G. A., Quock, M., Slangen, A. B. A., & Törnqvist, T. E. (2023). River Deltas and Sea-Level Rise. *Annual Reviews of Earth and Planetary Sciences*, *51*, 79–104. https://doi.org/10.1146/annurev-earth-031621

Olliver, E. A., Edmonds, D. A., & Shaw, J. B. (2020). Influence of Floods, Tides, and Vegetation on Sediment Retention in Wax Lake Delta, Louisiana, USA. *Journal of Geophysical Research: Earth Surface*, *125*(1), 1–21. https://doi.org/10.1029/2019JF005316

Orton, G. J., & Reading, H. G. (1993). Variability of deltaic processes in terms of sediment supply, with particular emphasis on grain size. *Sedimentology*, *40*, 475–512.

Overeem, I., Nienhuis, J. H., & Piliouras, A. (2022, April 1). Ice-dominated Arctic deltas. *Nature Reviews Earth and Environment*. Springer Nature. https://doi.org/10.1038/s43017-022-00268-x

Paniagua-Arroyave, J. F., Adams, P. N., Parra, S. M., & Valle-Levinson, A. (2019). Observations of surface-gravity-wave scattering and dissipation by an isolated shoal related to a cuspate foreland. *Continental Shelf Research*, *173*, 43–55. https://doi.org/10.1016/j.csr.2018.12.004

Paola, C., Twilley, R. R., Edmonds, D. A., Kim, W., Mohrig, D., Parker, G., et al. (2011). Natural processes in delta restoration: Application to the Mississippi Delta. *Annual Review of Marine Science*, *3*, 67–91. https://doi.org/10.1146/annurev-marine-120709-142856

Passalacqua, P., Lanzoni, S., Paola, C., & Rinaldo, A. (2013). Geomorphic signatures of deltaic processes and vegetation: The Ganges-Brahmaputra-Jamuna case study. *Journal of Geophysical Research: Earth Surface*, *118*(3), 1838–1849. https://doi.org/10.1002/jgrf.20128

Patruno, S., & Helland-Hansen, W. (2018, October 1). Clinoforms and clinoform systems: Review and dynamic classification scheme for shorelines, subaqueous deltas, shelf edges and continental margins. *Earth-Science Reviews*. Elsevier B.V. https://doi.org/10.1016/j.earscirev.2018.05.016

Piccardi, M., Correa, I. D., & Pranzini, E. (2020). Cispatá Bay and Mestizos Evolution as Reconstructed from Old Documents and Maps (16th–20th Century). *Journal of Marine Science and Engineering*, *8*(9), 1–27. https://doi.org/10.3390/jmse8090669

Postma, G. (1995). Causes of architectural variation in deltas. In M. N. Oti & G. Postma (Eds.), *Geology of Deltas* (pp. 3–16). Rotterdam, The Netherlands: A.A. Balkema.

Reading, H. G., & Richards, M. (1994). Turbidite systems in deep-water basin margins classified by grain size and feeder system. *American Association of Petroleum Geologists Bulletin*, *78*(5), 792–822. https://doi.org/10.1306/a25fe3bf-171b-11d7-8645000102c1865d

Restrepo, J. D., & López, S. A. (2008). Morphodynamics of the Pacific and Caribbean deltas of Colombia, South America. *Journal of South American Earth Sciences*, *25*(1), 1–21. https://doi.org/10.1016/j.jsames.2007.09.002

Saito, Y., Yang, Z., & Hori, K. (2001). The Huanghe (Yellow River) and Changjiang (Yangtze River) deltas: a review on their characteristics, evolution and sediment discharge during the Holocene. *Geomorphology*, *41*(2–3), 219–231. https://doi.org/10.1016/S0169-555X(01)00118-0

Sassi, M. G., Hoitink, A. J. F., de Brye, B., Vermeulen, B., & Deleersnijder, E. (2011). Tidal impact on the division of river discharge over distributary channels in the Mahakam Delta. *Ocean Dynamics*, *61*(12), 2211–2228. https://doi.org/10.1007/s10236-011-0473-9

Serrano Suarez, B. E. (2004). The Sinú river delta on the northwestern Caribbean coast of Colombia: Bay infilling associated with delta development. *Journal of South American Earth Sciences*, *16*(7), 623–631. https://doi.org/10.1016/j.jsames.2003.10.005

Seybold, H., Andrade, J. S., & Herrmann, H. J. (2007). Modeling river delta formation. *Proceedings of the National Academy of Sciences of the United States of America*, *104*(43), 16804–16809. https://doi.org/10.1073/pnas.0705265104

Shaw, J. B., Mohrig, D., & Whitman, S. K. (2013). The morphology and evolution of channels on the Wax Lake Delta, Louisiana, USA. *Journal of Geophysical Research: Earth Surface*, *118*(3), 1562–1584. https://doi.org/10.1002/jgrf.20123

Syvitski, J. P. M., & Milliman, J. D. (2007). Geology, Geography, and Humans Battle for Dominance over the Delivery of Fluvial Sediment to the Coastal Ocean. *The Journal of Geology*, *115*(1), 1–19. https://doi.org/10.1086/509246

Törnqvist, T. E., Wallace, D. J., Storms, J. E. A., Wallinga, J., van Dam, R. L., Blaauw, M., et al. (2008). Mississippi Delta subsidence primarily caused by compaction of Holocene strata. *Nature Geoscience*, *1*(3), 173–176. https://doi.org/10.1038/ngeo129

Valle-Levinson, A. (2010). Definition and classification of estuaries. In A. Valle-Levinson (Ed.), *Contemporary Issues in Estuarine Physics* (pp. 1–11). Cambridge, UK: Cambridge University Press.

Wang, H., Saito, Y., Zhang, Y., Bi, N., Sun, X., & Yang, Z. (2011, September). Recent changes of sediment flux to the western Pacific Ocean from major rivers in East and Southeast Asia. *Earth-Science Reviews*. https://doi.org/10.1016/j.earscirev.2011.06.003

Winterwerp, J. C., Graaff, R. F. de, Groeneweg, J., & Luijendijk, A. P. (2007). Modelling of wave damping at Guyana mud coast. *Coastal Engineering*, *54*(3), 249–261. https://doi.org/10.1016/J.COASTALENG.2006.08.012

Wolinsky, M. A., Edmonds, D. A., Martin, J., & Paola, C. (2010). Delta allometry: Growth laws for river deltas. *Geophysical Research Letters*, *37*(21), 1–6. https://doi.org/10.1029/2010GL044592

Woodroffe, C. D., Nicholls, R. J., Saito, Y., Chen, Z., & Goodbred, S. L. (2006). Landscape Variability and the Response of Asian Megadeltas to Environmental Change. In N. Harvey (Ed.), *Global Change and Integrated Coastal Management: The Asia-Pacific Region* (Vol. 10, pp. 277–314). Dordrecht, The Netherlands: Springer.

Wright, L. D. (1977). Sediment transport and deposition at river mouths: A synthesis. *Bulletin of the Geological Society of America*, *88*(6), 857–868. https://doi.org/10.1130/0016-7606(1977)88<857:STADAR>2.0.CO;2

Wright, L. D., & Coleman, J. M. (1971). Effluent expansion and interfacial mixing in the presence of a Salt Wedge, Mississippi River Delta. *Journal of Geophysical Research*, *76*(36), 8649–8661. https://doi.org/10.1029/JC076i036p08649

Wright, L. D., & Coleman, J. M. (1972). River Delta Morphology: Profile, Wave Climate and the Role of the Subaqueous. *Science*, *176*, 1–4.

Wright, L. D., & Coleman, J. M. (1973). Variations in morphology of major river deltas as functions on ocean wave and river discharge regimes. *American Association of Petroleum Geologists Bulletin*, *57*(2), 370–398.

Xu, K., Bentley, S. J., Day, J. W., & Freeman, A. M. (2019). A review of sediment diversion in the Mississippi River Deltaic Plain. *Estuarine, Coastal and Shelf Science*, *225*. https://doi.org/10.1016/j.ecss.2019.05.023

Zhang, W., Xu, Y. J., Guo, L., Lam, N. S. N., Xu, K., Yang, S., et al. (2022). Comparing the Yangtze and Mississippi River Deltas in the light of coupled natural-human dynamics: Lessons learned and implications for management. *Geomorphology*, *399*, 108075. https://doi.org/10.1016/J.GEOMORPH.2021.108075